STAR-RIS Assisted Secure MIMO Communication Networks: Transmit Power Minimization for Perfect and Imperfect CSI

Meng Shen, Xianfu Lei, *Member, IEEE*, Xiangyun Zhou, *Fellow, IEEE*, and George K. Karagiannidis, *Fellow, IEEE*

***Abstract*—In this paper, we investigate the secure transmission design for simultaneously transmitting and reflecting reconfigurable intelligent surface (STAR-RIS)-assisted multiple-input multiple-output (MIMO) systems. By considering both perfect and imperfect channel state information (CSI) scenarios, we jointly optimize the covariance matrix of the transmitter and the transmitting and reflecting coefficients of the STAR-RIS and formulate two transmit power minimization problems. For the optimization problem in the perfect CSI scenario, we develop a penalty-based alternating optimization (AO) algorithm to handle it. For the optimization problem in the imperfect CSI scenario, this paper is the first work to study the robust beamforming design for STAR-RIS-assisted secure MIMO systems. To address this challenging problem, we first use the inequalities of the determinant to transform it into an equivalent form. Then, we use the generalized S-procedure to handle the worst-case constraints. Finally, we develop a penalty-based AO algorithm. Performance evaluation results show that the two proposed optimization algorithms significantly reduce the transmit power compared to other baseline schemes.**

***Index Terms*—Reconfigurable intelligent surface, multiple-input multiple-output, simultaneously transmitting and reflecting, physical layer security, robust design.**

I. Introduction

RECONFIGURABLE intelligent surface (RIS) is considered as a promising new technology to increase the capacity of sixth generation (6G) wireless communication systems while reducing the operating cost of 6G wireless communication systems [1]. In particular, it enables end-to-end wireless channel reconfiguration by employing numerous low-cost and low-power passive elements. By adjusting the phase shift pattern of each passive element, the electromagnetic waves are reflected in the desired directions, thus improving the performance of the systems [2]–[6]. In addition, the use of RIS is also able to improve the physical layer security of communication systems [7]–[11]. The reason is that we can appropriately program RIS to degrade the eavesdropper's channel. For example, [7] and [8] have investigated the RIS-assisted secure communication systems and focused their attentions on maximizing the secrecy rate. Artificial noise has been employed to improve the security of the RIS-assisted communication systems in [9] and [10]. In [11], a RIS-aided multiple-multiple-input multiple-output (MIMO) secure communication system has been presented. However, both studies simply assume that channel state information (CSI) is perfect. By considering imperfect CSI, there are some works investigating robust transmission design [12]–[17]. For example, the authors of [12] have focused on multiple RISs-assisted secure communication systems. In [13] and [14], RIS-assisted secure multiple-input single-output (MISO) communications have been studied using alternating optimization (AO) approaches. In another effort, a robust transmission scheme aiming at maximizing the system sum rate for self-sustaining RIS-assisted MISO communication systems has been proposed in [15].

It should be noted that the above works [7]–[17] assume that the ability of the RIS is to reflect the incident signal, i.e., they consider the reflection-only RIS. Therefore, it has a requirement on the location of the transmitter and receiver, e.g., their geographical locations must be on the same side of the RIS. However, this geographical limitation may not always be satisfied in practice, which seriously restricts the flexible use of RIS. To overcome this limitation, the novel concept of simultaneously transmitting and reflecting RIS (STAR-RIS) has been proposed [18]–[20]. Unlike the reflecting-only RIS, the STAR-RIS is capable of transmitting and reflecting the incident signal simultaneously, thus providing 360° coverage, which allows the STAR-RIS to be flexible. To achieve both reflection and transmission, each STAR-RIS element supports both electric polarization and magnetization currents. Similar to the reflection-only RIS, the signal can be reconfigured by designing the transmitting and reflecting coefficients, thereby controlling the propagation of the wireless signal. Inspired by the benefits of STAR-RIS, several works have focused on the design of the transmission scheme [21]–[25]. For example, in [21], the authors have considered a STAR-RIS-assisted MISO system and studied the maximization of the weighted sum secrecy rate. In [22], the authors have considered a downlink and focused their attentions on maximizing the achievable sum rate. A STAR-RIS-assisted secure Internet of Medical Things

The work was in part supported by the National Natural Science Foundation of China under Grant 62271420 and Grant U23A20273. (*Corresponding author: Xianfu Lei.*)

Meng Shen and Xianfu Lei are with the School of Information Science and Technology, Southwest Jiaotong University, Chengdu 610031, China (email: mengshen@my.swjtu.edu.cn; xflei@swjtu.edu.cn).

Xiangyun Zhou is with the School of Engineering, The Australian National University, Canberra, ACT 2601, Australia (e-mail: xiangyun.zhou@anu.edu.au).

George K. Karagiannidis is with the Department of Electrical and Computer Engineering, Aristotle University of Thessaloniki, 541 24 Thessaloniki, Greece and also with the Cyber Security Systems and Applied AI Research Center, Lebanese American University (LAU), Beirut 1102-2801, Lebanon (e-mail: geokarag@auth.gr).

scheme aimed at achieving efficient e-health data transmission and maximizing secrecy energy efficiency has been proposed in [23]. In [24], the authors have studied a STAR-RIS-assisted uplink NOMA network, where the maximization of the minimum secrecy capacity under the full eavesdropping CSI scenario and the minimization of the maximum secrecy loss probability (SOP) under the statistical eavesdropping CSI scenario have been investigated. In addition, in [25], the authors have studied the MISO STAR-RIS-assisted NOMA downlink networks, where their focus is on maximizing the energy efficiency (EE).

It should be emphasized that the results presented in [21]–[25] are not applicable to the STAR-RIS-assisted MIMO systems, since the constraints of MIMO systems are in the form of logarithmic determinants rather than the logarithmic scalar form of MISO systems. In fact, to the best of our knowledge, there is an initial work dedicated to the secure STAR-RIS-assisted MIMO transmissions [26]. Specifically, the authors of [26] have investigated the weighted sum rate maximization problem for STAR-RIS-assisted MIMO networks, where a block coordinate descent algorithm is developed. We note that this existing work did not consider the security of the physical layer, although it is an important issue for STAR-RIS-assisted MIMO systems. Furthermore, we note that this work made the simplifying assumption that the perfect CSI is available. However, it is difficult to obtain the perfect CSI in STAR-RIS-assisted MIMO systems because the STAR-RIS is not equipped with radio frequency (RF) chains. Overall, to the best of our knowledge, the problem of how to effectively utilize STAR-RIS to ensure the secure transmission of MIMO systems has not been investigated in the literature. In an effort to address this open problem, in this paper, we study a STAR-RIS-assisted MIMO system in which the energy splitting (ES) protocol is considered. For such a system, we present a novel secure transmission scheme while minimizing the transmit power under both perfect and imperfect CSI scenarios. Within this framework, the main contributions of this paper can be summarized as follows:

- We investigate the joint design of the transmit covariance matrix and the transmitting and reflecting coefficients to minimize the transmit power in a STAR-RIS-assisted MIMO system under the perfect CSI scenario. The problem is intractable due to the non-convexity of the constraints and the coupling of the optimization variables. To solve it, an efficient algorithm is developed using the AO method. In particular, the successive convex approximation (SCA) technique and a penalty approach are used within the framework of the algorithm.
- To the best of our knowledge, this is the first work that focuses on the worst-case robust transmission design for STAR-RIS-assisted MIMO secure systems. It is also a non-convex optimization problem. Compared with the optimization problem in the perfect CSI scenario, this problem is more difficult to solve because the determinant functions include the uncertainties of the CSI. To address this, we first use the inequalities of the determinant to transform it into an equivalent form. Then, we apply the generalized S-procedure to handle the CSI uncertainties constraints. Finally, an efficient algorithm is developed by using the penalty-based AO method.
- The performance evaluation results show the superiority of the proposed schemes compared to other secure transmission schemes that either use conventional RIS or use RIS with random transmission and reflection coefficients. In particular, the performance evaluation results show that the proposed schemes significantly reduce the transmit power.

The remainder of the paper is organized as follows. After this introduction, Section II presents the system model. In Section III, the transmit power minimization problem is formally introduced when perfect CSI is available and an AO algorithm is proposed as an effective solution. In Section IV, the same problem is formulated when imperfect CSI of reflection channels is considered and a solution based upon the AO algorithm is presented. Section V gives various performance evaluation results, and Section VI summarizes this paper.

Notations: Boldface lower-case letter represents vectors. Boldface upper-case letter represents matrices. $\mathbb{C}^{M\times N}$ and $\mathbb{H}^M$ denote the set of $M\times N$ complex-valued matrices and of $M\times M$ Hermitian matrices, respectively. $\mathbf{1}_m$ is an $m\times 1$ vector with all entries 1. $\mathbf{I}_M$ denotes the identity matrix with M rows and M columns. When $\mathbf{X}$ is a square matrix, Rank($\mathbf{X}$), Tr($\mathbf{X}$), $(\mathbf{X})^{-1}$, $|\mathbf{X}|$ and $\mathbf{X}^H$ refer to the rank, trace of matrix $\mathbf{X}$, inverse of matrix $\mathbf{X}$, determinant of $\mathbf{X}$ and conjugate transpose of matrix $\mathbf{X}$, respectively. x_i stands for the i^{th} element of vector $\mathbf{x}$. $||\mathbf{X}||_2$ represents the spectral norm of matrix $\mathbf{X}$. $||\mathbf{X}||_*$ refers to the nuclear norm of matrix $\mathbf{X}$. $||\mathbf{X}||_F$ refers to the Frobenius norm of matrix $\mathbf{X}$. The diagonal matrix whose principal diagonal elements are taken from the vector $\mathbf{x}$ is denoted as diag($\mathbf{x}$). Diag($\mathbf{X}$) denotes a vector whose elements are taken from the principal diagonal elements of the matrix $\mathbf{X}$. $\lambda_{max}(\mathbf{X})$ and $\boldsymbol{\lambda}_{\max}(\mathbf{X})$ represent the largest eigenvalue of matrix $\mathbf{X}$ and the corresponding eigenvector of the largest eigenvalue, respectively. $\mathbf{X}\succeq\mathbf{0}$ indicates that $\mathbf{X}$ is a positive semidefinite matrix; $\mathbf{X}^\dagger$ and $\mathbf{X}^\star$ refer to the optimal value; $\mathbb{E}(\cdot)$ denotes the expectation operation. The block diagonal matrix with diagonal components $\mathbf{Z}_1,\cdots,\mathbf{Z}_n$ is represented by $\mathrm{blkdiag}(\mathbf{Z}_1,\cdots,\mathbf{Z}_n)$. $\mathcal{O}(\cdot)$ is the big-O notation.

II. System Model

As shown in Fig. 1, we consider a STAR-RIS-assisted secure MIMO communication network, where a multi-antenna Alice sends a message to two multi-antenna Bobs and a multi-antenna Eve tries to decode Bob's message. We make an assumption that obstacles block the direct communication links[1]. To enable communication, a STAR-RIS with M elements is deployed to provide the signal coverage for the geographically restricted Bobs. From the viewpoint of the STAR-RIS, the service area is divided into two regions, referred to as the

[1]If the direct links are available, the proposed optimization framework in the paper can be extended. In particular, one can use the block matrix to convert and represent the received signals in the presence of direct links in a form similar to these in this paper.

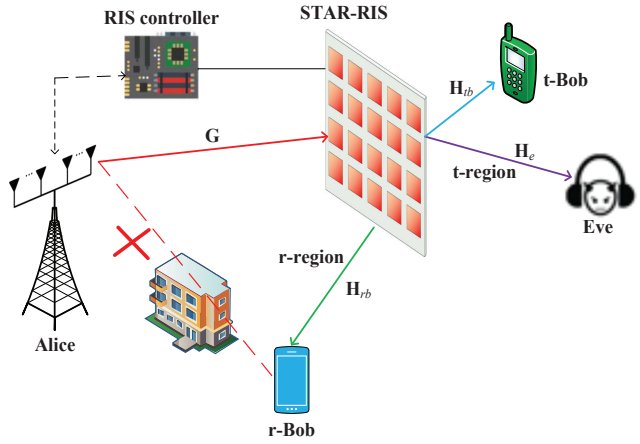

Fig. 1. A STAR-RIS-assisted secure MIMO communication network.

transmission region (t-region) and the reflection region (r-region), respectively. The Bob located in the transmission region is referred to as the t-Bob, while the Bob located in the reflection region is referred to as r-Bob. We assume that Eve is located in the t-region[2]. Let $\mathbf{G} \in \mathbb{C}^{M\times N}$, $\mathbf{H}_{tb} \in \mathbb{C}^{N_{tb}\times M}$, $\mathbf{H}_e \in \mathbb{C}^{N_e\times M}$, and $\mathbf{H}_{rb} \in \mathbb{C}^{N_{rb}\times M}$ denote the low-pass equivalent channels between Alice and STAR-RIS, STAR-RIS and the t-Bob, STAR-RIS and Eve, STAR-RIS and r-Bob, respectively, where N, N_{lb}, and N_e are the numbers of antennas for Alice, the l-Bob, $l \in \Pi = \{t, r\}$, and the Eve, respectively. In addition, we focus on the study of ES protocol of STAR-RIS, that is, the power of the incident signal is split to serve t-Bob and r-Bob simultaneously.

In this paper, we make an assumption that Alice sends the same messages to the t-Bob and r-Bob[3]. Let us denote $\mathbf{x} \in \mathbb{C}^{N\times 1}$ as the transmit signal with $\mathbb{E}\{\mathbf{x}\mathbf{x}^H\} = \mathbf{Q} \in \mathbb{C}^{N\times N}$, where $\mathbf{Q} \succeq 0$ denotes the transmit covariance matrix of the Alice. Hence, the signal received at the l-Bob, $\mathbf{y}_{lb}$, and Eve, $\mathbf{y}_e$, are given, respectively, by

$$\mathbf{y}_{lb} = \mathbf{H}_{lb}\mathbf{\Phi}_l\mathbf{G}\mathbf{x} + \mathbf{n}_{lb}, \tag{1}$$

$$\mathbf{y}_e = \mathbf{H}_e\mathbf{\Phi}_t\mathbf{G}\mathbf{x} + \mathbf{n}_e, \tag{2}$$

where $\mathbf{\Phi}_t = \mathrm{diag}\left(\sqrt{\alpha_1^t}e^{j\phi_1^t}, \sqrt{\alpha_2^t}e^{j\phi_2^t}, \ldots, \sqrt{\alpha_M^t}e^{j\phi_M^t}\right)$ and $\mathbf{\Phi}_r = \mathrm{diag}\left(\sqrt{\alpha_1^r}e^{j\phi_1^r}, \sqrt{\alpha_2^r}e^{j\phi_2^r}, \ldots, \sqrt{\alpha_M^r}e^{j\phi_M^r}\right)$ denote the transmission and reflection coefficient matrices, respectively, while $\mathbf{n}_{lb} \sim \mathcal{CN}\left(\mathbf{0}, \sigma_{lb}^2\mathbf{I}\right)$ and $\mathbf{n}_e \sim \mathcal{CN}\left(\mathbf{0}, \sigma_e^2\mathbf{I}\right)$ refer to the additive white Gaussian noise (AWGN) at the l-Bob and Eve, respectively, where σ_{lb}^2 and σ_e^2 are the associated average noise power.

Accordingly, the secrecy capacity (when it is positive) of l-Bob can be expressed as

$$C_{sec,l} = R_{lb} - R_e, \tag{3}$$

[2]Here we consider a typical outdoor-to-indoor communication scenario, which consists of a transmitter (Alice), an outdoor user (r-Bob), an indoor user (t-Bob), an indoor untrusted user (Eve), and a STAR-RIS deployed on the surface of the building.

[3]Since Alice sends the same messages to the t-Bob and r-Bob, the algorithms proposed in this paper can be easily extended to the multiple Bob scenarios.

where R_{lb} and R_{te} denote the channel capacity for the l-Bob and Eve, respectively, and are given by

$$R_{lb} = \log_2\left|\mathbf{I} + \frac{1}{\sigma_{lb}^2}\mathbf{H}_{lb}\mathbf{\Phi}_l\mathbf{G}\mathbf{Q}\mathbf{G}^H\mathbf{\Phi}_l^H\mathbf{H}_{lb}^H\right|, \tag{4}$$

$$R_e = \log_2\left|\mathbf{I} + \frac{1}{\sigma_e^2}\mathbf{H}_e\mathbf{\Phi}_t\mathbf{G}\mathbf{Q}\mathbf{G}^H\mathbf{\Phi}_t^H\mathbf{H}_{te}^H\right|. \tag{5}$$

III. Algorithm Design for STAR-RIS-Assisted Secure MIMO Communications With Perfect CSI

In this section, the transmit power minimization problem under the perfect CSI scenario[4] is formulated. Then, a solution to this problem will be obtained.

A. Problem Formulation

Considering the perfect CSI scenario, the transmit power minimization problem can be formulated as

$$\min_{\mathbf{Q},\mathbf{\Phi}_l} \quad \mathrm{Tr}\left(\mathbf{Q}\right) \tag{6a}$$

$$\text{s.t.} \quad \min\left\{R_{lb}\right\} \geq T_b, \quad \forall l \in \Pi, \tag{6b}$$

$$\min\left\{C_{sec,l}\right\} \geq T_s, \quad \forall l \in \Pi, \tag{6c}$$

$$\phi_m^l \in [0, 2\pi), \quad \forall l \in \Pi, 1 \leq m \leq M, \tag{6d}$$

$$\sum_l \alpha_m^l = 1, \quad \forall l \in \Pi, 1 \leq m \leq M, \tag{6e}$$

$$\mathbf{Q} \succeq 0, \tag{6f}$$

where T_b and T_s in (6b) and (6c) denote the target overall achievable rate and secrecy rate[5], respectively. Constraint (6d) represents the feasible set of phase-shift coefficients. Constraint (6e) ensures that the law of conservation of energy holds.

By defining $\bar{\mathbf{H}}_{lb} = \frac{1}{\sigma_{lb}}\mathbf{H}_{lb}$ and $\bar{\mathbf{H}}_e = \frac{1}{\sigma_e}\mathbf{H}_e$ and applying mathematical operations, the problem (6) is reformulated as

$$\min_{\mathbf{Q},\mathbf{\Phi}_l} \quad \mathrm{Tr}\left(\mathbf{Q}\right) \tag{7a}$$

$$\text{s.t.} \quad \log_2\left|\mathbf{I} + \bar{\mathbf{H}}_{lb}\mathbf{\Phi}_l\mathbf{G}\mathbf{Q}\mathbf{G}^H\mathbf{\Phi}_l^H\bar{\mathbf{H}}_{lb}^H\right| \geq T_b, \quad \forall l \in \Pi, \tag{7b}$$

$$\log_2\left|\mathbf{I} + \bar{\mathbf{H}}_e\mathbf{\Phi}_t\mathbf{G}\mathbf{Q}\mathbf{G}^H\mathbf{\Phi}_t^H\bar{\mathbf{H}}_e^H\right| \leq T_e, \tag{7c}$$

$$(6d), (6e), (6f), \tag{7d}$$

where $T_e = T_b - T_s$. Note that problem (7) is non-convex on account of the highly-coupled $\mathbf{Q}$, $\mathbf{\Phi}_t$ and $\mathbf{\Phi}_r$ in constraints (7b), (7c) and the non-convex feasible set in constraint (6d).

[4]In practical scenarios, it is difficult to obtain perfect CSI. Therefore, the performance results obtained in this section provide an upper bound.

[5]Here we consider a more generalized scenario where Alice transmits both a secret message and a non-secret message to Bobs, where a wiretap code is used to encode both the secret message at a rate of $R_{lb} - R_{te}$ and the non-secrete message at a rate of R_{te}. Then, the overall rate of both messages is R_{lb}. Bob's achievable rate is R_{lb} which is enough for decoding both the secret and non-secret messages. The non-secrete message acts as redundancy in terms of protecting the secret message against Eve. We consider this generalized scenario which is in line with [12], [14], [16]. If the non-secret message is removed, then one can simply set $T_b = T_s$ in (6b) without changing the problem formulation.

In general, it is computationally intractable to obtain a globally optimal solution to problem (7). To address this, we propose a suboptimal AO algorithm that can obtain an efficient solution with polynomial time complexity. In particular, problem (7) is decomposed into the subproblem of optimizing the transmit covariance matrix and the subproblem of optimizing the transmitting and reflecting coefficients. In the process of solving subproblems, the SCA technique is adopted, as described below.

B. Optimizing the Transmit Covariance Matrix

When $\{\mathbf{\Phi}_t, \mathbf{\Phi}_r\}$ is fixed, we can obtain

$$\min_{\mathbf{Q}} \quad \mathrm{Tr}\left(\mathbf{Q}\right) \tag{8a}$$

$$\text{s.t.} \quad (7\text{b}), (7\text{c}), (6\text{f}). \tag{8b}$$

However, problem (8) is non-convex owing to the constraint (7c). Observing the constraint (7c), we find that its left-hand-side is a concave function. To overcome it, we use the first-order Taylor approximation method and obtain the upper bound of the expression $\log_2\left|\mathbf{I}+\bar{\mathbf{H}}_e\mathbf{\Phi}_t\mathbf{G}\mathbf{Q}\mathbf{G}^{\mathbf{H}}\mathbf{\Phi}_t^H\bar{\mathbf{H}}_e^H\right|$, as shown below.

Lemma 1: Let $\mathbf{Q}^{(n)}$ be any feasible point, then a linear upper bound of $\log_2\left|\mathbf{I}+\bar{\mathbf{H}}_e\mathbf{\Phi}_t\mathbf{G}\mathbf{Q}\mathbf{G}^{\mathbf{H}}\mathbf{\Phi}_t^H\bar{\mathbf{H}}_e^H\right|$ is expressed as

$$\begin{aligned}&\log_2\left|\mathbf{I}+\bar{\mathbf{H}}_e\mathbf{\Phi}_t\mathbf{G}\mathbf{Q}^{(n)}\mathbf{G}^H\mathbf{\Phi}_t^H\bar{\mathbf{H}}_e^H\right|\\&+\mathrm{Tr}\left[\frac{1}{\ln 2}\left(\mathbf{I}+\bar{\mathbf{H}}_e\mathbf{\Phi}_t\mathbf{G}\mathbf{Q}^{(n)}\mathbf{G}^H\mathbf{\Phi}_t^H\bar{\mathbf{H}}_e^H\right)^{-1}\right.\\&\qquad\left.\times\,\bar{\mathbf{H}}_e\mathbf{\Phi}_t\mathbf{G}(\mathbf{Q}-\mathbf{Q}^{(n)})\mathbf{G}^H\mathbf{\Phi}_t^H\bar{\mathbf{H}}_e^H\right].\end{aligned} \tag{9}$$

Proof: Since $\ln|\mathbf{Y}|$ is a differentiable concave function, using first-order Taylor approximation, we can obtain

$$\ln|\mathbf{Y}|\le\ln\left|\mathbf{Y}^{(n)}\right|+\mathrm{Tr}\left(\left(\frac{\partial(\ln|\mathbf{Y}|)}{\partial\mathbf{Y}}\right)_{\mathbf{Y}=\mathbf{Y}^{(n)}}(\mathbf{Y}-\mathbf{Y}^{(n)})\right), \tag{10}$$

where $\mathbf{Y}^{(n)}$ is a feasible point.

By applying the inequality (10) and $\partial(\ln|\mathbf{Y}|)=\mathrm{Tr}(\mathbf{Y}^{-1}\partial\mathbf{Y})$, a linear upper bound of $\ln\left|\mathbf{I}+\bar{\mathbf{H}}_e\mathbf{\Phi}_t\mathbf{G}\mathbf{Q}\mathbf{G}^H\mathbf{\Phi}_t^H\bar{\mathbf{H}}_e^H\right|$ is

$$\begin{aligned}&\ln\left|\mathbf{I}+\bar{\mathbf{H}}_e\mathbf{\Phi}_t\mathbf{G}\mathbf{Q}\mathbf{G}^H\mathbf{\Phi}_t^H\bar{\mathbf{H}}_e^H\right|\\&\le\ln\left|\mathbf{I}+\bar{\mathbf{H}}_e\mathbf{\Phi}_t\mathbf{G}\mathbf{Q}^{(n)}\mathbf{G}^H\mathbf{\Phi}_t^H\bar{\mathbf{H}}_e^H\right|\\&+\mathrm{Tr}\left[\left(\mathbf{I}+\bar{\mathbf{H}}_e\mathbf{\Phi}_t\mathbf{G}\mathbf{Q}^{(n)}\mathbf{G}^H\mathbf{\Phi}_t^H\bar{\mathbf{H}}_e^H\right)^{-1}\right.\\&\qquad\left.\times\,\bar{\mathbf{H}}_e\mathbf{\Phi}_t\mathbf{G}(\mathbf{Q}-\mathbf{Q}^{(n)})\mathbf{G}^H\mathbf{\Phi}_t^H\bar{\mathbf{H}}_e^H\right].\end{aligned} \tag{11}$$

By applying mathematical operations, the proof is complete. ■

With the aid of Lemma 1, we can replace the constraint (7c) with the following form:

$$\begin{aligned}&\log_2\left|\mathbf{I}+\bar{\mathbf{H}}_e\mathbf{\Phi}_t\mathbf{G}\mathbf{Q}^{(n)}\mathbf{G}^H\mathbf{\Phi}_t^H\bar{\mathbf{H}}_e^H\right|\\&+\mathrm{Tr}\left[\frac{1}{\ln 2}\left(\mathbf{I}+\bar{\mathbf{H}}_e\mathbf{\Phi}_t\mathbf{G}\mathbf{Q}^{(n)}\mathbf{G}^H\mathbf{\Phi}_t^H\bar{\mathbf{H}}_e^H\right)^{-1}\right.\\&\qquad\left.\times\,\bar{\mathbf{H}}_e\mathbf{\Phi}_t(\mathbf{G}\mathbf{Q}\mathbf{G}^H-\mathbf{G}\mathbf{Q}^{(n)}\mathbf{G}^H)\mathbf{\Phi}_t^H\bar{\mathbf{H}}_e^H\right]\le T_e.\end{aligned} \tag{12}$$

By substituting (12) into the optimization problem (8), the following approximated reformulation can be given as

$$\min_{\mathbf{Q}} \quad \mathrm{Tr}\left(\mathbf{Q}\right) \tag{13a}$$

$$\text{s.t.} \quad (7\text{b}), (12), (6\text{f}). \tag{13b}$$

Problem (13) constitutes a convex problem. Hence, we can use the CVX tool to solve it [27].

C. Optimizing the Transmitting and Reflecting Coefficients

When $\mathbf{Q}$ is fixed, the transmitting and reflecting coefficients optimization subproblem is given by

$$\text{Find} \quad \mathbf{\Phi}_l \tag{14a}$$

$$\text{s.t.} \quad (7\text{b}), (7\text{c}), (6\text{d}), (6\text{e}). \tag{14b}$$

The main obstacle to solving the above problem lies in the non-convex feasible phase shift set constraint and energy conservation law constraint on the principal diagonal elements of $\mathbf{\Phi}_l$. In order to tackle it effectively, we adopt $\mathbf{v}_l=\mathrm{diag}(\mathbf{\Phi}_l)$ as the optimization variable instead of $\mathbf{\Phi}_l$ itself, and then reformulate problem (14). To start with, we focus on the reformulation of constraint (7b). Since $\mathbf{G}\mathbf{Q}\mathbf{G}^H$ is a Hermitian matrix, by performing the eigenvalue decomposition, we have

$$\mathbf{G}\mathbf{Q}\mathbf{G}^H=\sum_{i=1}^{s}\mathbf{p}_i\mathbf{p}_i^H, \tag{15}$$

where s is the number of non-zero eigenvalues. Then, we obtain

$$\begin{aligned}\bar{\mathbf{H}}_{lb}\mathbf{\Phi}_l\mathbf{G}\mathbf{Q}\mathbf{G}^H\mathbf{\Phi}_l^H\bar{\mathbf{H}}_{lb}^H&=\sum_{i=1}^{s}\bar{\mathbf{H}}_{lb}\mathbf{\Phi}_l\mathbf{p}_i\mathbf{p}_i^H\mathbf{\Phi}_l^H\bar{\mathbf{H}}_{lb}^H\\&=\sum_{i=1}^{s}\bar{\mathbf{H}}_{lb}\mathrm{diag}(\mathbf{p}_i)\mathbf{v}_l\mathbf{v}_l^H\mathrm{diag}(\mathbf{p}_i^H)\bar{\mathbf{H}}_{lb}^H.\end{aligned} \tag{16}$$

Thus, constraint (7b) can be rewritten as

$$\log_2\left|\mathbf{I}+\sum_{i=1}^{s}\bar{\mathbf{H}}_{lb}\mathrm{diag}(\mathbf{p}_i)\mathbf{v}_l\mathbf{v}_l^H\mathrm{diag}(\mathbf{p}_i^H)\bar{\mathbf{H}}_{lb}^H\right|\ge T_b,\quad\forall l\in\Pi. \tag{17}$$

Similarly, constraint (7c) can be rewritten as

$$\log_2\left|\mathbf{I}+\sum_{i=1}^{s}\bar{\mathbf{H}}_{e}\mathrm{diag}(\mathbf{p}_i)\mathbf{v}_t\mathbf{v}_t^H\mathrm{diag}(\mathbf{p}_i^H)\bar{\mathbf{H}}_{e}^H\right|\le T_e. \tag{18}$$

Based on the above discussions, problem (14) can be recast as

$$\text{Find} \quad \mathbf{v}_l \tag{19a}$$
$$\text{s.t.} \quad (17), (18), (6d), (6e). \tag{19b}$$

Problem (19) is still non-convex. To effectively solve it, we define $\mathbf{V}_l = \mathbf{v}_l \mathbf{v}_l^H, l \in \Pi$. Thus, problem (19) is rewritten as

$$\text{Find} \quad \mathbf{V}_l \tag{20a}$$
$$\text{s.t.} \quad \log_2 \left| \mathbf{I} + \mathbf{H}_{l1} \hat{\mathbf{V}}_l \mathbf{H}_{l1}^H \right| \geq T_b, \quad \forall l \in \Pi, \tag{20b}$$
$$\log_2 \left| \mathbf{I} + \mathbf{H}_{t2} \hat{\mathbf{V}}_t \mathbf{H}_{t2}^H \right| \leq T_e, \tag{20c}$$
$$\text{Rank}(\mathbf{V}_l) = 1, \quad \forall l \in \Pi, \tag{20d}$$
$$\text{diag}(\mathbf{V}_r + \mathbf{V}_t) = \mathbf{1}_M, \tag{20e}$$

where $\mathbf{H}_{l1} = \left[\bar{\mathbf{H}}_{lb}\text{diag}(\mathbf{p}_1), \cdots, \bar{\mathbf{H}}_{lb}\text{diag}(\mathbf{p}_s)\right]$, $\mathbf{H}_{t2} = \left[\bar{\mathbf{H}}_{e}\text{diag}(\mathbf{p}_1), \cdots, \bar{\mathbf{H}}_{e}\text{diag}(\mathbf{p}_s)\right]$, $\hat{\mathbf{V}}_l = \text{blkdiag}(\underbrace{\mathbf{V}_l, \cdots, \mathbf{V}_l}_{s})$. Note that problem (20) remains non-convex due to the constraints (20c) and (20d). Firstly, we handle the constraint (20c). Since constraints (20c) and (7c) have a similar mathematical form, we handle the constraint (20c) in a similar way to handle the constraint (7c) and employ the SCA method. Specially, the constraint (20c) is reformulated as

$$\log_2 \left| \mathbf{I} + \mathbf{H}_{t2} \hat{\mathbf{V}}_t^{(n)} \mathbf{H}_{t2}^H \right| + \text{Tr}\left[\frac{1}{\ln 2} \left(\mathbf{I} + \mathbf{H}_{t2} \hat{\mathbf{V}}_t^{(n)} \mathbf{H}_{t2}^H \right)^{-1} \mathbf{H}_{t2} (\hat{\mathbf{V}}_t - \hat{\mathbf{V}}_t^{(n)}) \mathbf{H}_{t2}^H \right] \leq T_e, \tag{21}$$

where $\hat{\mathbf{V}}_t^{(n)}$ is a feasible point.

Furthermore, we consider the non-convex constraint (20d). To deal with it, a useful lemma is formally introduced as follows.

Lemma 2: If $\mathbf{Y}$ is a Hermitian matrix, then $\text{Rank}(\mathbf{Y}) = 1$ is equivalent to

$$\|\mathbf{Y}\|_* - \|\mathbf{Y}\|_2 \leq 0, \tag{22}$$

where $\|\mathbf{Y}\|_* = \sum_j \delta_j$, $\|\mathbf{Y}\|_2 = \max_j \{\delta_j\}$ and δ_j is the j^{th} singular value of $\mathbf{Y}$.

Proof: Since $\|\mathbf{Y}\|_* - \|\mathbf{Y}\|_2 \geq 0$, then

$$\|\mathbf{Y}\|_* - \|\mathbf{Y}\|_2 \leq 0 \Leftrightarrow \|\mathbf{Y}\|_* - \|\mathbf{Y}\|_2 = 0 \Leftrightarrow \text{rank}(\mathbf{Y}) = 1. \tag{23}$$

■

With the aid of Lemma 2, constraint (20d) can be equivalently represented as follows

$$||\mathbf{V}_l||_* - ||\mathbf{V}_l||_2 \leq 0, \quad \forall l \in \Pi. \tag{24}$$

Substituting (21) and (24) into (20), we have

$$\text{Find} \quad \mathbf{V}_l \tag{25a}$$
$$\text{s.t.} \quad (20b), (20e), (21), (24). \tag{25b}$$

It is noted that problem (25) remains non-convex owing to the d.c. form constraint (24). In order to circumvent this difficulty, we here adopt a penalty-based method [28, Ch. 17].

Algorithm 1 SCA Algorithm for Obtaining $\mathbf{\Phi}_l^\dagger$

1: Initialize $\mathbf{V}_t^{(0)}$ with M random phases and M random amplitudes, initialize $\mathbf{V}_r^{(0)}$ with M random phases and M random amplitudes, and obtain $\hat{\mathbf{V}}_t^{(0)}$ by applying $\hat{\mathbf{V}}_t^{(0)} = \text{blkdiag}(\underbrace{\mathbf{V}_t^{(0)}, \cdots, \mathbf{V}_t^{(0)}}_{s})$. Set the iteration number $n = 0$ and accuracy $0 \leq \varepsilon \ll 1$;
2: **repeat**
3: For given $\mathbf{V}_t^{(n)}$, $\mathbf{V}_r^{(n)}$, and $\hat{\mathbf{V}}_t^{(n)}$, update $\mathbf{V}_t^{(n+1)}$, $\mathbf{V}_r^{(n+1)}$ as the optimal solution of problem (28), and obtain $\hat{\mathbf{V}}_t^{(n+1)}$;
4: Set $n \to n+1$;
5: **until** $|C(\mathbf{V}_l^{(n+1)}) - C(\mathbf{V}_l^{(n)})| \leq \varepsilon$.
6: $\mathbf{V}_l^\dagger = \mathbf{V}_l^{(n+1)}$.
7: Recover $\mathbf{\Phi}^\dagger$ from $\mathbf{V}_l^\dagger$ by performing Cholesky decomposition.

In particular, we move the constraint (24) into the objective function and then have

$$\min_{\mathbf{V}_l} \quad \sum_{l \in \Pi} \rho \left(||\mathbf{V}_l||_* - ||\mathbf{V}_l||_2 \right) \tag{26a}$$
$$\text{s.t.} \quad (20b), (20e), (21). \tag{26b}$$

In (26), ρ is a non-negative penalty factor that is used to penalize the violation of constraint (24). The proof of equivalence of problems (25) and (26) resorts to the following proposition.

Proposition 1: Given a penalty factor ρ_q, we obtain the optimal solutions $\mathbf{V}_{t_q}$ and $\mathbf{V}_{r_q}$ by solving problem (26). When the value of ρ_q is large enough, i.e., $\rho_q \to \infty$, the limit points $\mathbf{V}_{t_q}$ and $\mathbf{V}_{r_q}$ of $\overline{\mathbf{V}}_t$ and $\overline{\mathbf{V}}_r$, i.e., $\mathbf{V}_{t_q} \to \overline{\mathbf{V}}_t$ and $\mathbf{V}_{r_q} \to \overline{\mathbf{V}}_r$, are the feasible solutions of problem (25).

Proof: See Appendix A. ■

Proposition 1 states the fact that if we give a large enough penalty factor ρ, by solving the problem (26), we can obtain rank-one solutions $\mathbf{V}_t$ and $\mathbf{V}_r$. In other words, by applying the Cholesky decomposition, i.e., $\mathbf{V}_t = \mathbf{v}_t \mathbf{v}_t^H$ and $\mathbf{V}_r = \mathbf{v}_r \mathbf{v}_r^H$, we can obtain the transmitting and reflecting coefficients $\mathbf{\Phi}_t$ and $\mathbf{\Phi}_t$. It is noted that the problem (26) remains non-convex attributed to the fact that it involves the d.c. objective function. To deal with it, we adopt a similar approach as for dealing with constraint (7c) and employ the SCA. In particular, a lower bound for $\sum_{l \in \{t,r\}} \rho \left(||\mathbf{V}_l||_* - ||\mathbf{V}_l||_2 \right)$ is obtained as

$$C(\mathbf{V}_l) = \sum_{l \in \{t,r\}} \rho \Bigg(||\mathbf{V}_l||_* - ||\mathbf{V}_l^{(n)}||_2 - \text{Tr}\left(\boldsymbol{\lambda}_{\max}\left(\mathbf{V}_l^{(n)} \right) \times \boldsymbol{\lambda}_{\max}^{\text{H}}\left(\mathbf{V}_l^{(n)} \right) \left(\mathbf{V}_l - \mathbf{V}_l^{(n)} \right) \right) \Bigg), \tag{27}$$

where $\mathbf{V}_t^{(n)}$ and $\mathbf{V}_r^{(n)}$ are feasible points.

Substituting (27) into problem (26), we have

$$\min_{\mathbf{V}_l} \quad C(\mathbf{V}_l) \tag{28a}$$
$$\text{s.t.} \quad (20b), (20e), (21). \tag{28b}$$

The above problem is now convex. Thus, we can use the CVX tool to solve it [27]. **Algorithm 1** sketches the SCA approach for problem (28). Note that **Algorithm 1** converges according to [29].

Algorithm 2 Penalty-Based AO Algorithm

1: Initialize $\mathbf{\Phi}_t^{(0)}$ with M random phases and M random amplitudes and initialize $\mathbf{\Phi}_r^{(0)}$ with M random phases and M random amplitudes. Set the iteration number $n = 0$ and accuracy $0 \leq \varepsilon \ll 1$;
2: **repeat**
3: For given $\mathbf{\Phi}_t^{(n)}$ and $\mathbf{\Phi}_r^{(n)}$, update $\mathbf{Q}^{(n)}$ by solving (13);
4: For given $\mathbf{Q}^{(n)}$, update $\mathbf{\Phi}_t^{(n+1)}$ and $\mathbf{\Phi}_r^{(n+1)}$ by applying **Algorithm 1**;
5: Set $n \to n+1$;
6: **until** $|\operatorname{Tr}\left(\mathbf{Q}^{(n+1)}\right) - \operatorname{Tr}\left(\mathbf{Q}^{(n)}\right)| \leq \varepsilon$.

D. Complexity and Convergence

Algorithm 2 reports the proposed algorithm for solving problem (7), and its convergence proof and complexity analysis are described below.

To start with, the convergence is demonstrated. Denote by $F\left(\mathbf{Q}, \mathbf{\Phi}_t, \mathbf{\Phi}_r\right)$ the objective value of problem (8). Then, we have

$$F\left(\mathbf{Q}^{(n)}, \mathbf{\Phi}_t^{(n)}, \mathbf{\Phi}_r^{(n)}\right) \overset{(a)}{=} F\left(\mathbf{Q}^{(n)}, \mathbf{\Phi}_t^{(n+1)}, \mathbf{\Phi}_r^{(n+1)}\right) \overset{(b)}{\geq} F\left(\mathbf{Q}^{(n+1)}, \mathbf{\Phi}_t^{(n+1)}, \mathbf{\Phi}_r^{(n+1)}\right). \tag{29}$$

In (29), the equality (a) holds since the value of $F\left(\mathbf{Q}, \mathbf{\Phi}_t, \mathbf{\Phi}_r\right)$ does not depend on $\mathbf{\Phi}_t$ and $\mathbf{\Phi}_r$, and also $\mathbf{\Phi}_t^{(n+1)}$, and $\mathbf{\Phi}_r^{(n+1)}$, and $\mathbf{Q}^{(n)}$ are feasible solutions for problem (7). The inequality (b) holds attributed to the fact that $\mathbf{Q}^{(n+1)}$ is the optimal solution of problem (8) with given $\mathbf{\Phi}_t^{(n+1)}$ and $\mathbf{\Phi}_r^{(n+1)}$.

According to [30, Th. 3.12], the general expression for the complexity of solving an SDP problem is

$$\mathcal{O}\left(m_{SDP} n_{SDP}^{7/2} + m_{SDP}^2 n_{SDP}^{5/2} + m_{SDP}^3 n_{SDP}^{1/2}\right). \tag{30}$$

In (30), m_{SDP} is the number of second-order cones whose dimension is n_{SDP}. For solving subproblem (13), the complexity is $\mathcal{O}\left(2N^{3.5} + 4N^{2.5} + 8N^{0.5}\right)$. For solving subproblem (28), the complexity is $\mathcal{O}\left(I_1(2M^{3.5} + 4M^{2.5} + 8M^{0.5})\right)$, wherein I_1 is the number of inner loop. Hence, the complexity of **Algorithm 2** is $\mathcal{O}\big(I_{AO}(2N^{3.5} + 2I_1M^{3.5} + 4N^{2.5} + 4I_1M^{2.5} + 8N^{0.5} + 8I_1M^{0.5}\big)$, wherein I_{AO} is the number of outer loop.

IV. Algorithm Design for STAR-RIS-Assisted Secure MIMO Communications With Imperfect CSI

In this section, firstly the CSI uncertainty model is introduced and then the transmit power minimization problem for the scenario where reflection CSI is imperfect is formulated. A solution to this problem will be obtained.

A. Channel State Information (CSI)

The estimation method for STAR-RIS-related channels is the same as that for RIS-related channels. In particular, when the cascade channel estimation approach is adopted [31]–[33], i.e., to estimate the cascaded Alice-STAR-RIS-Bob channels, the training overhead is high. Therefore, it is a great challenge for practical applications. To overcome this obstacle, separate channel estimation approach is adopted [34], i.e., to estimate the Alice-STAR-RIS channel and STAR-RIS-Bob channels separately. Fortunately, since the location of STAR-RIS is usually fixed, the angles of arrival and departure change slowly. By calculating them, we can obtain the accurate CSI of the Alice-STAR-RIS channel. By comparison, the accurate CSI of the STAR-RIS-Bob channel is difficult to obtain because Bob is usually a mobile user and the STAR-RIS has limited signal processing capabilities. To account for the inevitable STAR-RIS-Bob channel estimation errors, a norm bound model is adopted [35]–[37]. In particular, $\mathbf{H}_{lb}$ and $\mathbf{H}_e$ are modeled as follows:

$$\begin{aligned}
&\mathbf{H}_{lb} = \widehat{\mathbf{H}}_{lb} + \Delta\mathbf{H}_{lb}, \\
&\Omega_{lb} = \left\{\Delta\mathbf{H}_{lb} \in \mathbb{C}^{N_{lb}\times M} : \|\Delta\mathbf{H}_{lb}\|_F \leq \xi_{lb}\right\}, \quad \forall l \in \Pi, \\
&\mathbf{H}_e = \widehat{\mathbf{H}}_e + \Delta\mathbf{H}_e, \\
&\Omega_e = \left\{\Delta\mathbf{H}_e \in \mathbb{C}^{N_e\times M} : \|\Delta\mathbf{H}_e\|_F \leq \xi_e\right\}.
\end{aligned} \tag{31}$$

B. Problem Formulation

With reference to (6) and (31), the optimization problem of transmit power minimization is formulated as follows:

$$\min_{\mathbf{Q}, \mathbf{\Phi}_l} \quad \operatorname{Tr}(\mathbf{Q}) \tag{32a}$$

$$\text{s.t.} \quad \min_{\Delta\mathbf{H}_{lb}\in\Omega_{lb}} \log_2\left|\mathbf{I} + \frac{1}{\sigma_{lb}^2}\mathbf{H}_{lb}\mathbf{R}_l\mathbf{H}_{lb}^H\right| \geq T_b, \forall l \in \Pi, \tag{32b}$$

$$\max_{\Delta\mathbf{H}_e\in\Omega_e} \log_2\left|\mathbf{I} + \frac{1}{\sigma_e^2}\mathbf{H}_e\mathbf{R}_t\mathbf{H}_e^H\right| \leq T_e, \tag{32c}$$

$$(6d), (6e), (6f), \tag{32d}$$

where $\mathbf{R}_l = \mathbf{\Phi}_l\mathbf{G}\mathbf{Q}\mathbf{G}^H\mathbf{\Phi}_l^H$. The logarithmic expressions for the determinants in the constraints (32b) and (32c) include infinitely many inequalities and as such they are non-convex. Thus, it is impossible to obtain a globally optimal solution to problem (32). To handle it, we propose a suboptimal AO algorithm with polynomial time complexity. Firstly, we introduce the following lemma.

Lemma 3: (Determinant Inequalities [38]) Let $\mathbf{Y}_1 \succ \mathbf{0}$, $\mathbf{Y}_2 \succeq \mathbf{0}, \mathbf{Y}_3 \preceq \mathbf{0}$, then $|\mathbf{Y}_1 + \mathbf{Y}_2| \geq |\mathbf{Y}_1|$ and $|\mathbf{Y}_1 + \mathbf{Y}_3| \leq |\mathbf{Y}_1|$.

By applying Lemma 3 and introducing slack optimization variables $\mathbf{D}_{1l} \in \mathbb{H}^{N_{lb}} \succeq 0$ and $\mathbf{D}_2 \in \mathbb{H}^{N_e} \succeq 0$, we replace the terms $\frac{1}{\sigma_{lb}^2}\mathbf{H}_{lb}\mathbf{\Phi}_l\mathbf{G}\mathbf{Q}\mathbf{G}^H\mathbf{\Phi}_l^H\mathbf{H}_{lb}^H$ and $\frac{1}{\sigma_e^2}\mathbf{H}_e\mathbf{\Phi}_t\mathbf{G}\mathbf{Q}\mathbf{G}^H\mathbf{\Phi}_t^H\mathbf{H}_e^H$ in the constraints (32b) and (32c), respectively, and obtain the following proposition.

Proposition 2: The equivalent form of problem (32) is as

Algorithm 3 SCA Algorithm for Obtaining $\mathbf{Q}^{\dagger}$

1: Initialize with a random $\mathbf{Q}^{(0)}$ and initialize with a random $\mathbf{D}_2^{(0)}$. Set the iteration number $n=0$ and accuracy $0 \leq \varepsilon \ll 1$;
2: **repeat**
3: For given $\mathbf{D}_2^{(n)}$, update $\mathbf{D}_2^{(n+1)}$ as the optimal solution of convex problem (38), and obtain $\mathbf{Q}^{(n+1)}$;
4: Set $n \to n+1$;
5: **until** $|\operatorname{Tr}\left(\mathbf{Q}^{(n+1)}\right) - \operatorname{Tr}\left(\mathbf{Q}^{(n)}\right)| \leq \varepsilon$.
6: $\mathbf{Q}^{\dagger} = \mathbf{Q}^{(n+1)}$.

follows:

$$\min_{\substack{\mathbf{Q},\mathbf{\Phi}_t,\mathbf{\Phi}_r \\ \mathbf{D}_{1t},\mathbf{D}_{1r},\mathbf{D}_2}} \quad \operatorname{Tr}(\mathbf{Q}) \tag{33a}$$

$$\text{s.t.} \quad \log_2|\mathbf{I}+\mathbf{D}_{1l}| \geq T_b, \quad \forall l \in \Pi, \tag{33b}$$

$$\log_2|\mathbf{I}+\mathbf{D}_2| \leq T_e, \tag{33c}$$

$$\frac{1}{\sigma_{lb}^2}(\widehat{\mathbf{H}}_{lb}+\triangle\mathbf{H}_{lb})\mathbf{R}_l(\widehat{\mathbf{H}}_{lb}^H+\triangle\mathbf{H}_{lb}^H) \succeq \mathbf{D}_{1l}, \quad \forall \triangle\mathbf{H}_{lb} \in \Omega_{lb}, \forall l \in \Pi, \tag{33d}$$

$$\frac{1}{\sigma_e^2}(\widehat{\mathbf{H}}_e+\triangle\mathbf{H}_e)\mathbf{R}_t(\widehat{\mathbf{H}}_e^H+\triangle\mathbf{H}_e^H) \preceq \mathbf{D}_2, \quad \forall \triangle\mathbf{H}_e \in \Omega_e, \tag{33e}$$

$$(6d), (6e), (6f). \tag{33f}$$

Proof: Please see Appendix B. ∎

Note that problem (33) is non-convex owing to the inclusion of non-convex constraints (33c)-(33e). It is observed that constraint (33c) is similar to constraint (7c) in the perfect CSI scenario, so we can handle it in a similar way. The constraints (33d) and (33e) are new constraints, which involve infinitely many inequalities owing to they contain continuous CSI's uncertain sets. Firstly, we handle constraints (33d) and (33e). To handle them, we resort to the lemma 4.

Lemma 4: (Generalized S-Procedure [39, Prop. 3.4]) Let $f(\mathbf{Y})$=$\mathbf{Y}^{\mathrm{H}}\mathbf{D}\mathbf{Y} + \mathbf{Y}^{\mathrm{H}}\mathbf{B} + \mathbf{B}^{\mathrm{H}}\mathbf{Y} + \mathbf{C}$ and $\mathbf{A} \succeq 0$. Then, $f(\mathbf{Y}) \succeq \mathbf{0}, \forall \mathbf{Y} \in \left\{\mathbf{Y} \mid \operatorname{Tr}\left(\mathbf{A}\mathbf{Y}\mathbf{Y}^{\mathrm{H}}\right) \leq 1\right\}$, is equivalent to the following form:

$$\begin{bmatrix} \mathbf{C} & \mathbf{B}^{\mathrm{H}} \\ \mathbf{B} & \mathbf{D} \end{bmatrix} - \eta \begin{bmatrix} \mathbf{I} & \mathbf{0} \\ \mathbf{0} & -\mathbf{A} \end{bmatrix} \succeq \mathbf{0},$$

where $\eta \geq 0$.

By applying Lemma 4, constraints (33d) and (33e) can be expressed as

$$\begin{bmatrix} \widehat{\mathbf{H}}_{lb}\mathbf{R}_l\widehat{\mathbf{H}}_{lb}^H - \sigma_{lb}^2\mathbf{D}_{1l} - \eta_{lb}\mathbf{I} & \widehat{\mathbf{H}}_{lb}\mathbf{R}_l \\ \mathbf{R}_l\mathbf{\Phi}_l^H\widehat{\mathbf{H}}_{lb}^H & \mathbf{R}_l + \eta_{lb}\xi_{lb}^{-2}\mathbf{I} \end{bmatrix} \succeq \mathbf{0}, \quad \forall l \in \Pi, \tag{34}$$

and

$$\begin{bmatrix} \sigma_e^2\mathbf{D}_2 - \widehat{\mathbf{H}}_e\mathbf{R}_t\widehat{\mathbf{H}}_e^H - \eta_e\mathbf{I} & -\widehat{\mathbf{H}}_e\mathbf{R}_t \\ -\mathbf{R}_t\widehat{\mathbf{H}}_e^H & -\mathbf{R}_t + \eta_e\xi_{te}^{-2}\mathbf{I} \end{bmatrix} \succeq \mathbf{0}, \tag{35}$$

respectively, where $\eta_{tb} \geq 0$, $\eta_{rb} \geq 0$, and $\eta_e \geq 0$.

Next, we handle the non-convex constraint (33c). Similar to use the method of handling constraint (7c), we have

$$\log_2\left|\mathbf{I}+\mathbf{D}_2^{(n)}\right| + \operatorname{Tr}\left[\frac{1}{\ln 2}(\mathbf{I}+\mathbf{D}_2^{(n)})^{-1}(\mathbf{D}_2-\mathbf{D}_2^{(n)})\right] \leq T_e, \tag{36}$$

Algorithm 4 SCA Algorithm for Obtaining $\mathbf{\Phi}_l^{\dagger}$

1: Initialize $\mathbf{V}_t^{(0)}$ with M random phases and M random amplitudes, initialize $\mathbf{V}_r^{(0)}$ with M random phases and M random amplitudes, initialize with a random $\mathbf{D}_2^{(0)}$. Set the iteration number $n=0$ and accuracy $0 \leq \varepsilon \ll 1$;
2: **repeat**
3: For given $\mathbf{V}_t^{(n)}$, $\mathbf{V}_r^{(n)}$, and $\mathbf{D}_2^{(n)}$, update $\mathbf{V}_t^{(n+1)}$, $\mathbf{V}_r^{(n+1)}$, and $\mathbf{D}_2^{(n+1)}$ as the optimal solutions of convex problem (41);
4: Set $n \to n+1$;
5: **until** $|C(\mathbf{V}_l^{(n+1)}) - C(\mathbf{V}_l^{(n)})| \leq \varepsilon$.
6: $\mathbf{V}_l^{\dagger} = \mathbf{V}_l^{(n+1)}$.
7: Recover $\mathbf{\Phi}_l^{\dagger}$ from $\mathbf{V}_l^{\dagger}$ by performing Cholesky decomposition.

Algorithm 5 Penalty-Based AO Algorithm

1: Initialize with a random $\mathbf{Q}^{(0)}$, initialize $\mathbf{\Phi}_t^{(0)}$ with M random phases and M random amplitudes, initialize $\mathbf{\Phi}_r^{(0)}$ with M random phases and M random amplitudes. Set the iteration number $n=0$ and accuracy $0 \leq \varepsilon \ll 1$;
2: **repeat**
3: For given $\mathbf{\Phi}_t^{(n)}$ and $\mathbf{\Phi}_r^{(n)}$, solve (38) by applying **Algorithm 3** and obtain $\mathbf{Q}^{(n+1)}$;
4: For given $\mathbf{Q}^{(n+1)}$, solve (41) by applying **Algorithm 4** and obtain $\mathbf{\Phi}_t^{(n+1)}$ and $\mathbf{\Phi}_r^{(n+1)}$;
5: Set $n \to n+1$;
6: **until** $|\operatorname{Tr}\left(\mathbf{Q}^{(n+1)}\right) - \operatorname{Tr}\left(\mathbf{Q}^{(n)}\right)| \leq \varepsilon$.

where $\mathbf{D}_2^{(n)}$ is a feasible point.

Finally, by substituting (34), (35) and (36), problem (33) becomes

$$\min_{\substack{\mathbf{Q},\mathbf{\Phi}_t,\mathbf{\Phi}_t \\ \mathbf{D}_{1t},\mathbf{D}_{1r},\mathbf{D}_2 \\ \eta_{tb},\eta_{rb},\eta_e}} \quad \operatorname{Tr}(\mathbf{Q}) \tag{37a}$$

$$\text{s.t.} \quad (6d), (6e), (6f), (33b), (34), (35), (36). \tag{37b}$$

However, problem (37) remains non-convex owing to the coupling of optimization variables. Motivated by the method applied to tackle problem (7), the AO method is extended to tackle problem (37).

C. Optimizing the Transmit Covariance Matrix

When $\{\mathbf{\Phi}_t, \mathbf{\Phi}_r\}$ is fixed, the problem of optimizing $\mathbf{Q}$ simplifies to

$$\min_{\substack{\mathbf{Q},\mathbf{D}_{1t} \\ \mathbf{D}_{1r},\mathbf{D}_2 \\ \eta_{tb},\eta_{rb},\eta_e}} \quad \operatorname{Tr}(\mathbf{Q}) \tag{38a}$$

$$\text{s.t.} \quad (6f), (33b), (34), (35), (36). \tag{38b}$$

Problem (38) is now convex. Thus, we can use the CVX tool to solve it [27]. **Algorithm 3** sketches the SCA approach for problem (38). Note that **Algorithm 3** converges according to [29].

D. Optimizing the Transmitting and Reflecting Coefficients

When $\mathbf{Q}$ is fixed, by performing the eigenvalue decomposition and applying $\mathbf{\Phi}_l\mathbf{p}_i = \operatorname{diag}(\mathbf{p}_i)\mathbf{v}_l$, constraints (34) and

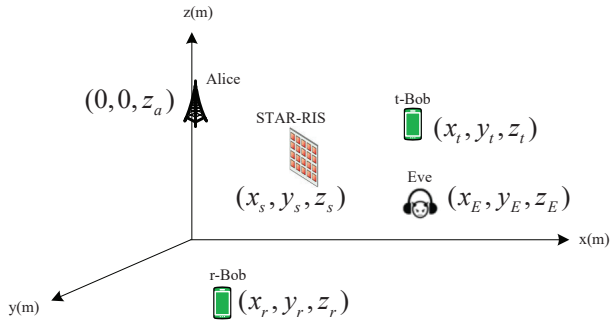

Fig. 2. The communication scenario setup.

(35) can be equivalently represented as

$$\begin{bmatrix} \widehat{\mathbf{H}}_{lb}\mathbf{U}_l\widehat{\mathbf{H}}_{lb}^H - \sigma_{lb}^2\mathbf{D}_{1l} - \eta_{lb}\mathbf{I} & \widehat{\mathbf{H}}_{lb}\mathbf{U}_l \\ \mathbf{U}_l\widehat{\mathbf{H}}_{lb}^H & \mathbf{U}_l + \eta_{lb}\xi_{lb}^{-2}\mathbf{I} \end{bmatrix} \succeq \mathbf{0}, \quad (39)$$

$$\begin{bmatrix} \sigma_e^2\mathbf{D}_2 - \widehat{\mathbf{H}}_e\mathbf{U}_t\widehat{\mathbf{H}}_e^H - \eta_e\mathbf{I} & -\widehat{\mathbf{H}}_e\mathbf{U}_t \\ -\mathbf{U}_t\widehat{\mathbf{H}}_e^H & -\mathbf{U}_t + \eta_e\xi_e^{-2}\mathbf{I} \end{bmatrix} \succeq \mathbf{0}, \quad (40)$$

respectively, where $\mathbf{U}_l = \sum_{i=1}^{s} \mathrm{diag}(\mathbf{p}_i)\mathbf{V}_l\mathrm{diag}(\mathbf{p}_i^H)$.

Then, similar to the previous section, by fixing $\mathbf{Q}$, the problem of optimizing $\mathbf{V}_l$ becomes

$$\min_{\substack{\mathbf{V}_t,\mathbf{V}_r \\ \mathbf{D}_{1t},\mathbf{D}_{1r},\mathbf{D}_2 \\ \eta_{tb},\eta_{rb},\eta_e}} \quad C(\mathbf{V}_l) \quad (41a)$$

$$\text{s.t.} \quad (33b), (36), (39), (40). \quad (41b)$$

It is noted that the above problem constitutes a convex problem. Thus, we can use the CVX tool to solve it [27]. **Algorithm 4** sketches the SCA approach for problem (41). Note that **Algorithm 4** converges according to [29].

E. Complexity and Convergence

Algorithm 5 summarizes the proposed algorithm for solving problem (41). In the inner loop for updating $\mathbf{Q}$, $\mathbf{\Phi}_t$ and $\mathbf{\Phi}_r$, the solutions which can guarantee convergence exist according to [29]. By applying a similar proof as for **Algorithm 2**, we can show that **Algorithm 5** converges. In addition, since both subproblems (38) and (41) are SDP problems, we can use (30) to calculate the complexity of **Algorithm 5**. In particular, the complexity of the SDP subproblem for the transmit covariance matrix optimization is $\mathcal{O}\left(I_2(4N^{3.5}+16N^{2.5}+64N^{0.5})\right)$, where I_2 is the iteration number. The complexity of the SDP subproblem for transmitting and reflecting coefficients optimization is $\mathcal{O}\left(I_3(4M^{3.5}+16M^{2.5}+64M^{0.5})\right)$, where I_3 is the iteration number. Thus, the total complexity of **Algorithm 5** is $\mathcal{O}\big(I_{ite}(I_2(4N^{3.5}+16N^{2.5}+64N^{0.5}) + I_3(4M^{3.5}+16M^{2.5}+64M^{0.5}))\big)$, where I_{ite} represents the alternating iteration number.

V. Performance Evaluation Results And Discussion

In this section, various performance evaluation results, obtained by means of Monte Carlo computer simulations will be presented. The communication scenario setup is illustrated in Fig. 2. Specifically, Alice is located on the z-axis, while STAR-RIS and Eve are randomly distributed in a three-dimensional coordinate network. r-Bob and t-Bob are also randomly distributed on both sides of the STAR-RIS. We will then detail the channel models. Following this, we will review the baseline schemes used for performance comparisons and subsequently present the convergence performance of the proposed algorithms. In the next four subsections, detailed performance comparisons will be presented, focusing on transmit power and secrecy outage probability.

TABLE I
Simulation Parameters

Path loss exponents of Alice-STAR-RIS channels β_{AI}, STAR-RIS-Bobs channels β_{RB}, and STAR-RIS-Eve channels β_{RE}	2.2 [15]
Rician factors of Alice-STAR-RIS channels K_{AI}, STAR-RIS-Bobs channels K_{RB}, and STAR-RIS-Eve channels K_{RE}	5 dB [6]
Noise power at Bobs, σ_{tp}^2 and σ_{rp}^2	-90 dBm [12]
Noise power at Eve, σ_e^2	-90 dBm [12]
Penalty factor, ρ	1000
Accuracy, ε	10^{-4}

A. Channel Models

The small-scale fading for all the STAR-RIS-related channels is modeled as Rician fading. As for the large-scale fading, a distance dependent path loss model is adopted. For example, the channel coefficient, $\mathbf{G}$, of the Alice-STAR-RIS channel shown in Fig. 1 can be mathematically expressed as

$$\mathbf{G} = \sqrt{\mathrm{PL}_0(\frac{d_{AI}}{d_0})^{-\beta_{AI}}}\left(\sqrt{\frac{K_{AI}}{K_{AI}+1}}\mathbf{G}^{\mathrm{LoS}} + \sqrt{\frac{1}{K_{AI}+1}}\mathbf{G}^{\mathrm{NLoS}}\right). \quad (42)$$

In the above equation, $\mathrm{PL}_0 = -30$ dB, $d_0 = 1$ m, K_{AI}, d_{AI} and β_{AI} denote the Rician factor, distance and path loss exponent, respectively. In addition, $\mathbf{G}^{\mathrm{NLoS}}$ is the non-light of sight (NLoS) component that is Rayleigh fading and $\mathbf{G}^{\mathrm{LoS}}$ is the deterministic line of sight (LoS) component, which is modeled as $\mathbf{G}^{\mathrm{LoS}} = \mathbf{a}_M(\nu^{AoA})\mathbf{a}_{N_p}^H(\nu^{AoD})$ with

$$\mathbf{a}_M(\nu^{AoA}) = \left[1, e^{j2\pi\frac{d}{\lambda}\sin\nu^{AoA}}, \cdots, e^{j2\pi\frac{d}{\lambda}(M-1)\sin\nu^{AoA}}\right]^T, \quad (43)$$

and

$$\mathbf{a}_{N_p}^H(\nu^{AoD}) = \left[1, e^{j2\pi\frac{d}{\lambda}\sin\nu^{AoD}}, \cdots, e^{j2\pi\frac{d}{\lambda}(N_p-1)\sin\nu^{AoD}}\right]^T. \quad (44)$$

In (43) and (44), d refers to the antenna separation distance, λ refers to the signal wavelength, and ν^{AoA} and ν^{AoD} refer to the angles of arrival and departure, respectively. It is assumed that $d/\lambda = 0.5$, and ν^{AoA} and ν^{AoD} are randomly distributed

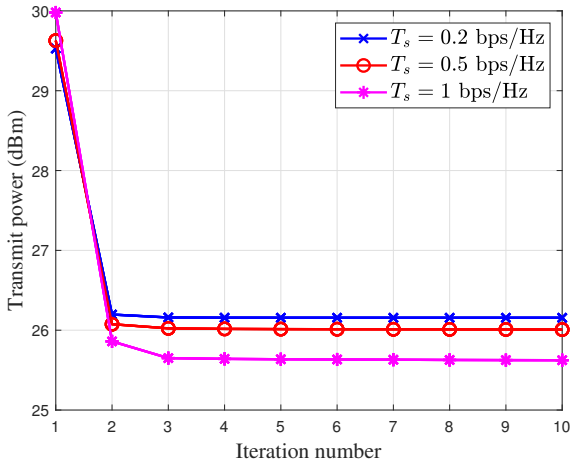

Fig. 3. Convergence of Algorithm 2.

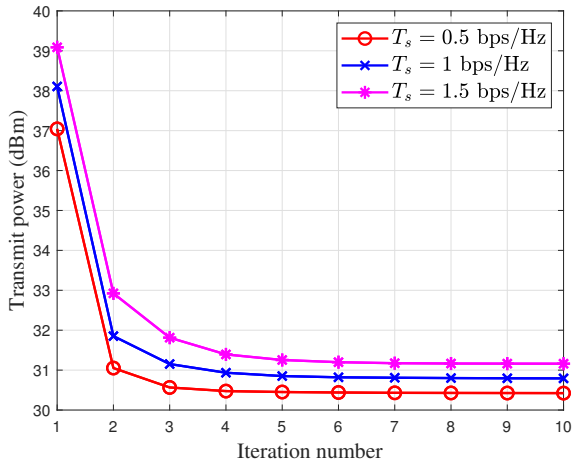

Fig. 4. Convergence of Algorithm 5.

within $[0, 2\pi]$ [40]. The channels from the STAR-RIS to t-Bob, the STAR-RIS to r-Bob, and the STAR-RIS to Eve can be modeled like $\mathbf{G}$ in (42). For the sake of presentation, we further assume that $\kappa_{tb} = \xi_{tb}/||\widehat{\mathbf{H}}_{tb}||_F$, $\kappa_{rb} = \xi_{rb}/||\widehat{\mathbf{H}}_{rb}||_F$, and $\kappa_e = \xi_e/||\widehat{\mathbf{H}}_e||_F$, where κ_{tb}, κ_{rb} and κ_e are defined as the normalized estimation error uncertainty of channels $\mathbf{H}_{tb}$, $\mathbf{H}_{rb}$ and $\mathbf{H}_e$, respectively [35]. For obtaining the various performance evaluation results which are reported latter on, the other simulation parameters are set as specified in Table I.

B. Baseline Schemes

The following two baseline schemes are provided for performance comparison with our proposed scheme.

- **Random amplitude/phase:** In this case, the transmitting and reflecting coefficients of STAR-RIS are not optimized and are randomly generated with satisfying $\phi_m^t, \phi_m^r \in [0, 2\pi)$ and $\alpha_m^t + \alpha_m^r = 1$. The transmit covariance matrix $\mathbf{Q}$ is optimized by solving problem (13) for the perfect CSI scenario and problem (38) for the imperfect CSI scenario, respectively.
- **Conventional RIS:** In this case, we deploy one conventional reflecting-only RIS and one transmitting-only RIS at the same position to provide a full-space coverage. For comparative fairness, both the reflecting-only RIS and the transmitting-only RIS are equipped with $\frac{M}{2}$ elements.

C. Convergence Performance

The convergence performance of Algorithms 2 and 5 has been evaluated and the results are shown in Figs. 3 and 4, respectively. The simulation parameters used for plotting Fig. 3 are set as $N = 6$, $N_{tb} = 2$, $N_{rb} = 2$, $N_e = 2$, $M = 30$, and $T_b = 2$ bps/Hz. Additionally, the locations of Alice, STAR-RIS, r-Bob, t-Bob and Eve used for plotting Fig. 3 are (0, 0, 10) m, (0, 100, 10) m, (0, 80, 2) m, (0, 120, 2) m and (3, 125, 2) m, respectively. The simulation parameters corresponding to Fig. 4 are set as $N = 3$, $N_{tb} = 2$, $N_{rb} = 2$, $N_e = 2$, $M = 16$, $T_b = 2.2$ bps/Hz, $\kappa_{tb} = 0.01$, $\kappa_{rb} = 0.01$ and $\kappa_e = 0.03$. Moreover, the coordinates for Alice, STAR-RIS, r-Bob, t-Bob, and Eve corresponding to Fig. 4 are given as (0, 0, 10) m, (0, 100, 10) m, (0, 90, 2) m, (0, 110, 2) m, and (3, 125, 2) m, respectively. It can be observed from both of figures that the transmit power is reduced when the target secrecy rate T_s decreases, which is expected since the security requirements of networks are reduced. In addition, the obtained results clearly confirm the convergence of Algorithms 2 and 5.

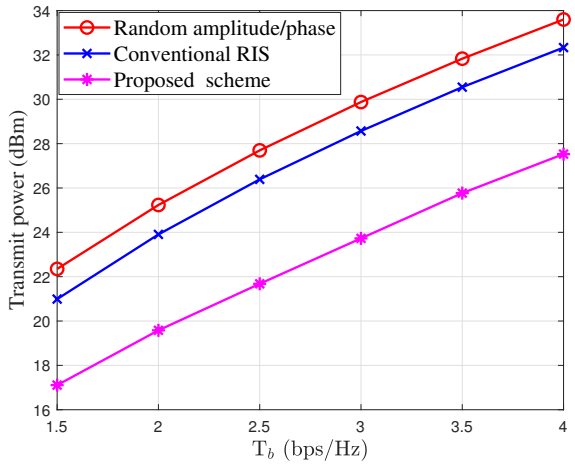

Fig. 5. Transmit power versus the target overall achievable rate with perfect CSI.

D. Transmit Power Versus the Target Overall Achievable Rate

The transmit power versus the target overall achievable rate, T_b, has been evaluated and the results are shown in Figs. 5 and 6, corresponding to the perfect CSI and imperfect CSI scenarios, respectively. The simulation parameters used for plotting Fig. 5 are set as $N = 5$, $N_{tb} = 5$, $N_{rb} = 2$, $N_e = 2$, $M = 20$, and $T_e = 1$ bps/Hz. Additionally, the locations of Alice, STAR-RIS, r-Bob, t-Bob and Eve used for plotting Fig. 5 are (0, 0, 10) m, (50, 0, 10) m, (30, 0, 2) m, (70, 0, 2) m and (55, 3, 2) m, respectively. The simulation parameters corresponding to Fig. 6 are set as $N = 4$, $N_{tb} = 2$,

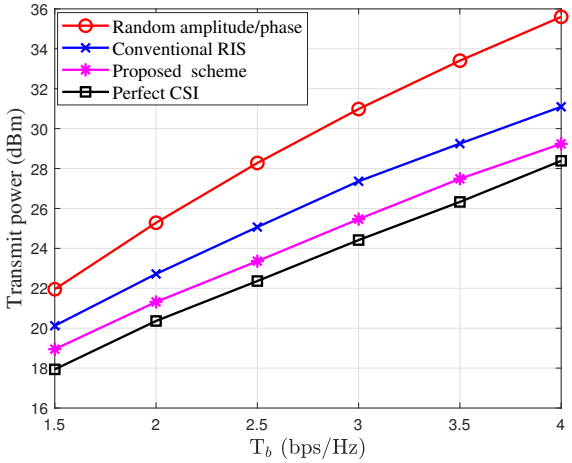

Fig. 6. Transmit power versus target overall achievable rate with imperfect CSI.

$N_{rb} = 2$, $N_e = 2$, $M = 16$, $T_e = 1$ bps/Hz, $\kappa_{tb} = 0.01$, $\kappa_{rb} = 0.01$ and $\kappa_e = 0.01$. Moreover, the coordinates for Alice, STAR-RIS, r-Bob, t-Bob, and Eve corresponding to Fig. 6 are given as (0, 0, 10) m, (35, 0, 10) m, (10, 0, 2) m, (55, 0, 2) m, and (50, 3, 2) m, respectively. It can be observed from Figs. 5 and 6 that transmit power increases gradually as the target overall achievable rate increases. This is because additional transmit power is required to satisfy the increased the target rate requirements of t-Bob and r-Bob. One can see that the proposed schemes for the perfect CSI and imperfect CSI scenarios require less transmit power than the random amplitude/phase scheme, which clearly underlines the importance of optimizing the transmitting and reflecting coefficients of STAR-RIS. The proposed schemes also outperform the conventional RIS scheme for both perfect CSI and imperfect CSI scenarios. The reason is that compared to the conventional RIS scheme, whose elements can only reflect or transmit the signal, the elements of STAR-RIS can simultaneously reflect and transmit the signal, therefore provide higher degrees-of-freedom to enhance the signal strength for t-Bob and r-Bob while simultaneously weakening Eve's signal strength. In addition, Fig. 6 also shows that the perfect CSI scheme requires the minimal transmit power, which provides a lower bound for the secure transmission scheme in the imperfect CSI scenario. Finally, using the same parameters as in Fig. 5 and setting $T_b = 3$, we study the tightness of the linear upper bound proposed in Lemma 1. As illustrated in Table II, we observe that the difference between the left-hand side of constraint (7c) and the linear upper bound in Lemma 1 is 4.13×10^{-5}. This shows that the proposed linear upper bound in Lemma 1 is very tight.

E. Transmit Power Versus the Number of STAR-RIS Elements

Considering the perfect CSI scenario, the transmit power versus the number of STAR-RIS elements, M, has been evaluated and the results are shown in Fig. 7. The simulation parameters used for plotting Fig. 7 are set as $N = 3$, $N_{tb} = 2$, $N_{rb} = 2$, $N_e = 2$, $T_b = 1.5$ bps/Hz, $T_s = 1$ bps/Hz.

TABLE II
COMPARISON BETWEEN THE PROPOSED LINEAR UPPER BOUND AND THE ACTUAL CHANNEL CAPACITY

$\log_2\left\|\mathbf{I}+\bar{\mathbf{H}}_e\mathbf{\Phi}_t\mathbf{G}\mathbf{Q}^{(n)}\mathbf{G}^H\mathbf{\Phi}_t^H\bar{\mathbf{H}}_e^H\right\|$ $+\mathrm{Tr}\left[\frac{1}{\ln 2}\left(\mathbf{I}+\bar{\mathbf{H}}_e\mathbf{\Phi}_t\mathbf{G}\mathbf{Q}^{(n)}\mathbf{G}^H\mathbf{\Phi}_t^H\bar{\mathbf{H}}_e^H\right)^{-1}\right.$ $\left.\times\bar{\mathbf{H}}_e\mathbf{\Phi}_t\mathbf{G}(\mathbf{Q}-\mathbf{Q}^{(n)})\mathbf{G}^H\mathbf{\Phi}_t^H\bar{\mathbf{H}}_e^H\right]$	0.5513341
$\log_2\left\|\mathbf{I}+\bar{\mathbf{H}}_e\mathbf{\Phi}_t\mathbf{G}\mathbf{Q}\mathbf{G}^{\mathbf{H}}\mathbf{\Phi}_t^H\bar{\mathbf{H}}_e^H\right\|$	0.5512928
Difference	4.13×10^{-5}

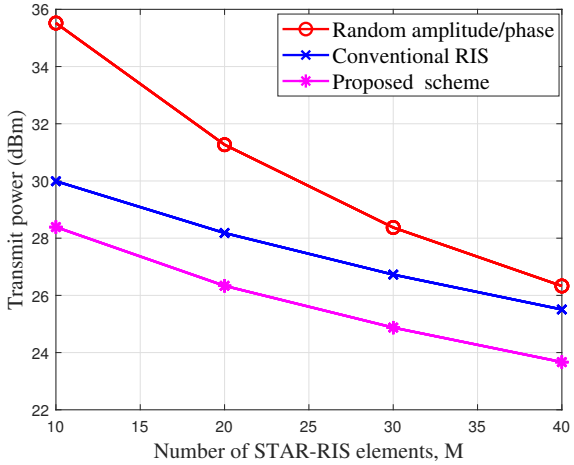

Fig. 7. Transmit power versus the number of STAR-RIS elements.

Additionally, the locations of Alice, STAR-RIS, r-Bob, t-Bob and Eve used for plotting Fig. 7 are (0, 0, 10) m, (0, 100, 10) m, (0, 85, 2) m, (0, 115, 2) m and (3, 115, 2) m, respectively. It can be observed from Fig. 7 that transmit power decreases gradually as the number of STAR-RIS elements increases. This phenomenon can be attributed to two facts. Firstly, by increasing the number of STAR-RIS elements, more signal can be captured by the STAR-RIS, resulting in a higher array gain. Secondly, by properly optimizing transmitting and reflecting coefficients, the signal power received at t-Bob and r-Bob can be enhanced while the signal power received at the Eve can be weakened. It is also noted that the proposed scheme requires less transmit power compared to the two baseline schemes, which again confirms the effectiveness of the proposed scheme.

F. CSI Uncertainty

Considering the imperfect CSI scenario, the transmit power performance versus the normalized estimation error uncertainty, κ, is studied in Fig. 8. We further assume $\kappa_{tb} = \kappa_{rb} = \kappa_e = \kappa$. The simulation parameters used for plotting Fig. 8 are set as $N = 4$, $N_{tb} = 2$, $N_{rb} = 2$, $N_e = 2$, $M = 10$, $T_b = 1.2$ bps/Hz, and $T_e = 1$ bps/Hz. Additionally, the locations of Alice, STAR-RIS, r-Bob, t-Bob and Eve are (0, 0, 10) m, (0, 100, 10) m, (0, 90, 2) m, (0, 110, 2) m and (3, 115, 2) m, respectively. It can be seen that the proposed scheme results in less transmit power compared to the random amplitude/phase scheme and conventional RIS

This article has been accepted for publication in IEEE Transactions on Communications. This is the author's version which has not been fully edited and content may change prior to final publication. Citation information: DOI 10.1109/TCOMM.2024.3430971

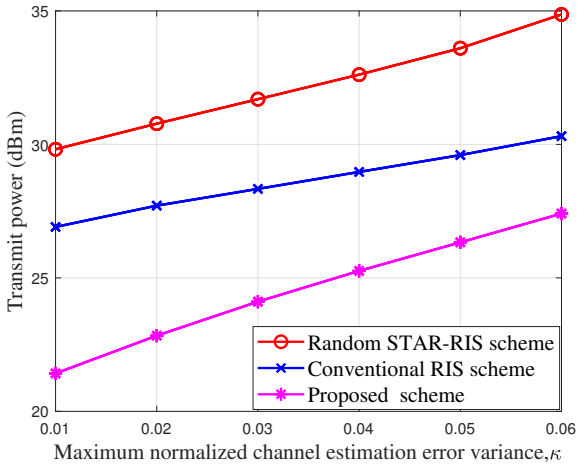

Fig. 8. Transmit power versus the normalized estimation error uncertainty.

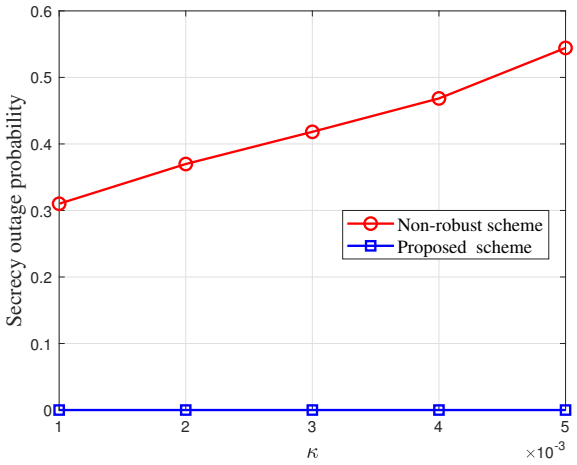

Fig. 9. Secrecy outage probability versus the normalized estimation error uncertainty, κ.

scheme, thereby demonstrating the advantage of the proposed scheme. Furthermore, as expected, the transmit power of the three schemes increases as the normalized estimation error uncertainty increases because in this case higher transmit power is needed to maintain the operational robustness. Fig. 9 plots the secrecy outage probability versus the normalized estimation error uncertainty κ. The secrecy outage probability is defined as the probability that the secrecy rate of t-bob or r-bob falls below a target rate. A non-robust scheme is provided for the performance comparison. For the non-robust scheme, the imperfect CSI is treated as perfect and then applying Algorithm 2 to optimize the transmit covariance matrix and the transmitting and reflecting coefficients. The simulation parameters used for plotting Fig. 9 are set as $N = 5$, $N_{tb} = 5$, $N_{rb} = 2$, $N_e = 2$, $M = 20$, $T_b = 3$ bps/Hz, and $T_e = 1$ bps/Hz. Additionally, the locations of Alice, STAR-RIS, r-Bob, t-Bob and Eve used for plotting Fig. 9 are (0, 0, 10) m, (50, 0, 10) m, (30, 0, 2) m, (70, 0, 2) m and (55, 3, 2) m, respectively. As can be seen from Fig. 9, the secrecy outage probability is zero, while that of the non-robust scheme is greater than 0.3, which emphasises the necessity of considering CSI estimation errors.

G. Impact of STAR-RIS Location

In Fig. 10, we study the impact of the STAR-RIS deployment on the transmit power performance in the imperfect CSI scenario. The STAR-RIS is located at (x_s, 1, 2) m, where x_s represents the horizontal coordinate and the range of x_s is set as $15 \leq x_s \leq 75$. The simulation parameters used for plotting Fig. 10 are set as $N = 3$, $N_{tb} = 2$, $N_{rb} = 2$, $N_e = 2$, $M = 20$, $T_b = 1.5$ bps/Hz, $T_e = 1$ bps/Hz, $\kappa_{tb} = 0.01$, $\kappa_{rb} = 0.01$ and $\kappa_e = 0.01$. Additionally, the locations of Alice, r-Bob, t-Bob and Eve used for plotting Fig. 10 are (0, 0, 3) m, (90, 0, -5) m, (90, 0, 5) m and (110, 0, 5) m, respectively. It can be observed from Fig. 10 that the transmit power required by all the schemes first increases and then decreases. This phenomenon is reasonable because the combined channel has the minimal channel gain when the STAR-RIS is located in

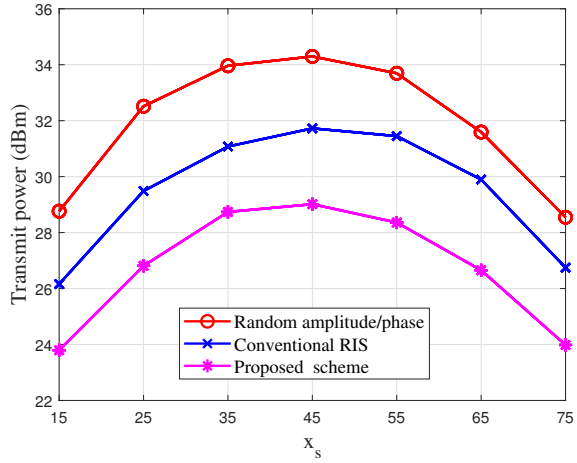

Fig. 10. Transmit power versus the STAR-RIS location.

the middle of Alice and Bobs. Furthermore, the proposed scheme requires less transmit power compared to the two baseline schemes, which again demonstrates the advantage of the proposed scheme.

VI. Conclusions

In this paper, we proposed secure transmission designs that minimize the transmit power of STAR-RIS-assisted MIMO systems operating in the presence of an external multi-antenna eavesdropper. By considering perfect CSI and imperfect CSI scenarios, we jointly optimized the transmit covariance matrix at the Alice and the transmitting and reflecting coefficients at the STAR-RIS, and formulated two optimization problems. Specifically, when perfect CSI is available, an efficient algorithm was proposed using the AO method. Within the framework of the algorithm, the SCA technique and a penalty method were used. Furthermore, for the imperfect CSI scenario, the formulated optimization problem is more intractable than the formulated optimization problem resulting from the perfect CSI scenario due to the CSI uncertainty

constraints. To solve it, we first used the inequalities of the determinant to transform it into an equivalent form. Then, we applied the generalized S-procedure to handle the CSI uncertainty constraints. Finally, a penalty-based AO algorithm was developed. The performance evaluation results verified the superiority of the proposed scheme compared to two other baseline schemes. The proposed algorithms can be extended to scenarios where multiple multi-antenna eavesdroppers and multiple multi-antenna Bob exist, which is the direction of our future research.

APPENDIX

A. Proof of Proposition 1

Given a penalty factor ρ_q, denote $g(\mathbf{V}_t, \mathbf{V}_r, \rho_q)$ as the objective function of problem (26) and $\mathbf{V}_{t_q}^\star$ and $\mathbf{V}_{r_q}^\star$ as their corresponding optimal solutions. Then, we have the following equality

$$g(\mathbf{V}_{t_q}^\star, \mathbf{V}_{r_q}^\star, \rho_q) = \rho_q \sum_{l\in\{t,r\}} \left(||\mathbf{V}_{l_q}^\star||_* - ||\mathbf{V}_{l_q}^\star||_2 \right). \quad (45)$$

By rearranging the above equality, we have

$$\sum_{l\in\{t,r\}} \left(||\mathbf{V}_{l_q}^\star||_* - ||\mathbf{V}_{l_q}^\star||_2 \right) = \frac{1}{\rho_q} g(\mathbf{V}_{t_q}^\star, \mathbf{V}_{r_q}^\star, \rho_q). \quad (46)$$

Suppose that $\overline{\mathbf{V}}_t^\star$ and $\overline{\mathbf{V}}_r^\star$ are limit points of the sequences $\mathbf{V}_{t_q}^\star$ and $\mathbf{V}_{r_q}^\star$, respectively. Then, an infinite subsequence $\mathcal{Q}$ can be found that satisfies

$$\lim_{q\in\mathcal{Q}} \mathbf{V}_{t_q}^\star = \overline{\mathbf{V}}_t^\star, \quad (47)$$

and

$$\lim_{q\in\mathcal{Q}} \mathbf{V}_{r_q}^\star = \overline{\mathbf{V}}_r^\star. \quad (48)$$

By taking the limit on both sides of the equality (46) , i.e., $q \in \mathcal{Q}, q \to \infty$, one can obtain

$$\begin{aligned} &\sum_{l\in\{t,r\}} (||\overline{\mathbf{V}}_l^\star||_* - ||\overline{\mathbf{V}}_l^\star||_2) \overset{(f)}{=} \lim_{q\in\mathcal{Q}} \sum_{l\in\{t,r\}} (||\mathbf{V}_{l_q}^\star||_* - ||\mathbf{V}_{l_q}^\star||_2) \\ &= \lim_{q\in\mathcal{Q}} \frac{1}{\rho_q} g(\mathbf{V}_{t_q}^\star, \mathbf{V}_{r_q}^\star) \overset{\rho_q\to\infty}{=} 0, \end{aligned} \quad (49)$$

where (f) holds because the functions $||\mathbf{V}_{t_q}^\star||_* - ||\mathbf{V}_{t_q}^\star||$ and $||\mathbf{V}_{r_q}^\star||_* - ||\mathbf{V}_{r_q}^\star||$ are continuous and the addition of two continuous functions is still a continuous function. Hence, one can obtain

$$\sum_{l\in\{t,r\}} (||\overline{\mathbf{V}}_l^\star||_* - ||\overline{\mathbf{V}}_l^\star||_2) = 0. \quad (50)$$

Based on the above equation, we conclude that $\overline{\mathbf{V}}_t^\star$ and $\overline{\mathbf{V}}_r^\star$ are the optimal solutions of problem (25).

Furthermore, let $\mathbf{V}_t^\star$ and $\mathbf{V}_r^\star$ be the optimal solutions of problem (25). Then, one can obtain

$$g(\mathbf{V}_t^\star, \mathbf{V}_r^\star, \rho_q) = 0. \quad (51)$$

As a result, $\mathbf{V}_t^\star$ and $\mathbf{V}_r^\star$ are the optimal solutions of problem (26). Based on the above discussion, the proof is completion.

B. Proof of Proposition 2

Denote $\mathbf{Q}^\dagger$, $\mathbf{\Phi}_t^\dagger$ and $\mathbf{\Phi}_r^\dagger$ the optimal solutions of problem (32), while $\mathbf{Q}^\star$, $\mathbf{\Phi}_t^\star$ and $\mathbf{\Phi}_r^\star$ denote the optimal solutions of problem (33). Since the expression of the objective functions for problems (32) and (33) is the same, we further denote the corresponding objective functions by $T(\mathbf{Q}, \mathbf{\Phi}_t, \mathbf{\Phi}_r)$. Since $\mathbf{Q}^\dagger$, $\mathbf{\Phi}_t^\dagger$, and $\mathbf{\Phi}_r^\dagger$ are the optimal solutions of problem (32), let

$$\mathbf{D}_{1l}^\dagger = \frac{1}{\sigma_{lb}^2} \mathbf{H}_{lb} \mathbf{\Phi}_l^\dagger \mathbf{G} \mathbf{Q}^\dagger \mathbf{G}^H (\mathbf{\Phi}_l^\dagger)^H \mathbf{H}_{lb}^H, \quad \forall l \in \Pi, \quad (52)$$

and

$$\mathbf{D}_{2t}^\dagger = \frac{1}{\sigma_e^2} \mathbf{H}_e \mathbf{\Phi}_t^\dagger \mathbf{G} \mathbf{Q}^\dagger \mathbf{G}^H (\mathbf{\Phi}_t^\dagger)^H \mathbf{H}_e^H. \quad (53)$$

According to equations (52) and (53), we conclude that $\mathbf{Q}^\dagger$, $\mathbf{\Phi}_t^\dagger$, and $\mathbf{\Phi}_r^\dagger$ are feasible solutions of problem (33). Then, we have

$$T\left(\mathbf{Q}^\dagger, \mathbf{\Phi}_t^\dagger, \mathbf{\Phi}_r^\dagger\right) \geq T\left(\mathbf{Q}^\star, \mathbf{\Phi}_t^\star, \mathbf{\Phi}_r^\star\right). \quad (54)$$

In addition, since $\mathbf{Q}^\star$, $\mathbf{\Phi}_t^\star$, and $\mathbf{\Phi}_r^\star$ are the optimal solutions of problem (33), one can obtain

$$\ln |\mathbf{I} + \mathbf{D}_{1l}^\star| \geq T_b, \quad \forall l \in \Pi, \quad (55)$$

and

$$\frac{1}{\sigma_{lb}^2} (\mathbf{H}_{lb} \mathbf{\Phi}_l^\star \mathbf{G} \mathbf{Q}^\star \mathbf{G}^H (\mathbf{\Phi}_l^\star)^H \mathbf{H}_{lb}^H) - \mathbf{D}_{1l}^\star \succeq \mathbf{0}, \quad \forall l \in \Pi, \quad (56)$$

where $\mathbf{D}_{1t}^\star$ and $\mathbf{D}_{1r}^\star$ are the optimal solutions of problem (33).

By applying Lemma 3, we can obtain

$$\left| \mathbf{I} + \frac{1}{\sigma_{lb}^2} (\mathbf{H}_{lb} \mathbf{\Phi}_l^\star \mathbf{G} \mathbf{Q}^\star \mathbf{G}^H (\mathbf{\Phi}_l^\star)^H \mathbf{H}_{lb}^H) \right| \geq |\mathbf{I} + \mathbf{D}_{1l}^\star|, \quad \forall l \in \Pi. \quad (57)$$

Then, we have

$$\log \left| \mathbf{I} + \frac{1}{\sigma_{lb}^2} (\mathbf{H}_{lb} \mathbf{\Phi}_l^\star \mathbf{G} \mathbf{Q}^\star \mathbf{G}^H (\mathbf{\Phi}_l^\star)^H \mathbf{H}_{lb}^H) \right| \geq T_b, \quad \forall l \in \Pi. \quad (58)$$

By using the same method, we have

$$\log \left| \mathbf{I} + \frac{1}{\sigma_e^2} \mathbf{H}_e \mathbf{\Phi}_t^\star \mathbf{G} \mathbf{Q}^\star \mathbf{G}^H (\mathbf{\Phi}_t^\star)^H \mathbf{H}_e^H \right| \leq T_e. \quad (59)$$

Combining (58) and (59), we conclude that $\mathbf{Q}^\star$, $\mathbf{\Phi}_t^\star$ and $\mathbf{\Phi}_r^\star$ are feasible solutions of problem (32). Then, we can obtain

$$T\left(\mathbf{Q}^\dagger, \mathbf{\Phi}_t^\dagger, \mathbf{\Phi}_r^\dagger\right) \leq T\left(\mathbf{Q}^\star, \mathbf{\Phi}_t^\star, \mathbf{\Phi}_r^\star\right). \quad (60)$$

Based on the above discussion, the proof is completion.

REFERENCES

[1] G. Zhou, C. Pan, H. Ren, K. Wang, and A. Nallanathan, "A framework of robust transmission design for IRS-aided MISO communications with imperfect cascaded channels," *IEEE Trans. Signal Process.*, vol. 68, pp. 5092–5106, 2020.

[2] M. Wu, X. Lei, X. Zhou, Y. Xiao, X. Tang, and R. Q. Hu, "Reconfigurable intelligent surface assisted spatial modulation for symbiotic radio," *IEEE Trans. Veh. Technol.*, vol. 70, no. 12, pp. 12 918–12 931, Dec. 2021.

[3] X. Lei, M. Wu, F. Zhou, X. Tang, R. Q. Hu, and P. Fan, "Reconfigurable intelligent surface-based symbiotic radio for 6G: Design, challenges, and opportunities," *IEEE Wireless Commun.*, vol. 28, no. 5, pp. 210–216, Oct. 2021.

[4] Q. Wu and R. Zhang, "Intelligent reflecting surface enhanced wireless network via joint active and passive beamforming," *IEEE Trans. Wireless Commun.*, vol. 18, no. 11, pp. 5394–5409, Nov. 2019.

[5] M. Shen, X. Lei, P. T. Mathiopoulos, and R. Q. Hu, "Robust beamforming design for IRS-aided secure communication systems under complete imperfect CSI," *IEEE Trans. Veh. Technol.*, vol. 72, no. 6, pp. 8204–8209, Jun. 2023.

[6] D. Xu, X. Yu, Y. Sun, D. W. K. Ng, and R. Schober, "Resource allocation for IRS-assisted full-duplex cognitive radio systems," *IEEE Trans. Commun.*, vol. 68, no. 12, pp. 7376–7394, Dec. 2020.

[7] X. Guan, Q. Wu, and R. Zhang, "Intelligent reflecting surface assisted secrecy communication: Is artificial noise helpful or not?" *IEEE Wireless Commun. Lett.*, vol. 9, no. 6, pp. 778–782, Jun. 2020.

[8] X. Yu, D. Xu, and R. Schober, "Enabling secure wireless communications via intelligent reflecting surfaces," in *Proc. IEEE Global Commun. Conf. (GLOBECOM)*, Dec. 2019, pp. 1–6.

[9] D. Xu, X. Yu, Y. Sun, D. W. K. Ng, and R. Schober, "Resource allocation for secure IRS-assisted multiuser MISO systems," in *Proc. IEEE Globecom Workshops (GC Wkshps)*, 2019, pp. 1–6.

[10] S. Hong, C. Pan, H. Ren, K. Wang, and A. Nallanathan, "Artificial-noise-aided secure MIMO wireless communications via intelligent reflecting surface," *IEEE Trans. Commun.*, vol. 68, no. 12, pp. 7851–7866, Dec. 2020.

[11] Z. Chu, W. Hao, P. Xiao, D. Mi, Z. Liu, M. Khalily, J. R. Kelly, and A. P. Feresidis, "Secrecy rate optimization for intelligent reflecting surface assisted MIMO system," *IEEE Trans. Inf. Forensics Secur.*, vol. 16, pp. 1655–1669, 2021.

[12] X. Yu, D. Xu, Y. Sun, D. W. K. Ng, and R. Schober, "Robust and secure wireless communications via intelligent reflecting surfaces," *IEEE J. Sel. Areas Commun.*, vol. 38, no. 11, pp. 2637–2652, Nov. 2020.

[13] X. Lu, W. Yang, X. Guan, Q. Wu, and Y. Cai, "Robust and secure beamforming for intelligent reflecting surface aided mmwave MISO systems," *IEEE Wireless Commun. Lett.*, vol. 9, no. 12, pp. 2068–2072, Dec. 2020.

[14] S. Hong, C. Pan, H. Ren, K. Wang, K. K. Chai, and A. Nallanathan, "Robust transmission design for intelligent reflecting surface-aided secure communication systems with imperfect cascaded CSI," *IEEE Trans. Wireless Commun.*, vol. 20, no. 4, pp. 2487–2501, Apr. 2021.

[15] S. Hu, Z. Wei, Y. Cai, C. Liu, D. W. K. Ng, and J. Yuan, "Robust and secure sum-rate maximization for multiuser MISO downlink systems with self-sustainable IRS," *IEEE Trans. Commun.*, vol. 69, no. 10, pp. 7032–7049, Oct. 2021.

[16] Z. Zhang, L. Lv, Q. Wu, H. Deng, and J. Chen, "Robust and secure communications in intelligent reflecting surface assisted NOMA networks," *IEEE Commun. Lett.*, vol. 25, no. 3, pp. 739–743, Mar 2021.

[17] H. Niu, Z. Chu, F. Zhou, Z. Zhu, L. Zhen, and K.-K. Wong, "Robust design for intelligent reflecting surface-assisted secrecy SWIPT network," *IEEE Trans. Wireless Commun.*, vol. 21, no. 6, pp. 4133–4149, Jun. 2022.

[18] Y. Liu, X. Mu, J. Xu, R. Schober, Y. Hao, H. V. Poor, and L. Hanzo, "STAR: Simultaneous transmission and reflection for 360° coverage by intelligent surfaces," *IEEE Wireless Commun.*, vol. 28, no. 6, pp. 102–109, Dec. 2021.

[19] X. Mu, Y. Liu, L. Guo, J. Lin, and R. Schober, "Simultaneously transmitting and reflecting (STAR) RIS aided wireless communications," *IEEE Trans. Wireless Commun.*, vol. 21, no. 5, pp. 3083–3098, May 2022.

[20] J. Xu, Y. Liu, X. Mu, and O. A. Dobre, "STAR-RISs: Simultaneous transmitting and reflecting reconfigurable intelligent surfaces," *IEEE Commun. Lett.*, vol. 25, no. 9, pp. 3134–3138, Sep. 2021.

[21] H. Niu, Z. Chu, F. Zhou, and Z. Zhu, "Simultaneous transmission and reflection reconfigurable intelligent surface assisted secrecy MISO networks," *IEEE Commun. Lett.*, vol. 25, no. 11, pp. 3498–3502, Nov. 2021.

[22] J. Zuo, Y. Liu, Z. Ding, L. Song, and H. V. Poor, "Joint design for simultaneously transmitting and reflecting (STAR) RIS assisted NOMA systems," *IEEE Trans. Wireless Commun.*, vol. 22, no. 1, pp. 611–626, Jan. 2023.

[23] W. Wang, W. Ni, H. Tian, Z. Yang, C. Huang, and K.-K. Wong, "Robust design for STAR-RIS secured internet of medical things," in *Proc. IEEE Int. Conf. Commun. Workshops (ICC Workshops)*, Jul. 2022, pp. 574–579.

[24] Z. Zhang, J. Chen, Y. Liu, Q. Wu, B. He, and L. Yang, "On the secrecy design of STAR-RIS assisted uplink NOMA networks," *IEEE Trans. Wireless Commun.*, vol. 21, no. 12, pp. 11 207–11 221, Dec. 2022.

[25] T. Wang, F. Fang, and Z. Ding, "Joint phase shift and beamforming design in a multi-user MISO STAR-RIS assisted downlink NOMA network," *IEEE Trans. Veh. Technol.*, pp. 1–12, 2023.

[26] H. Niu, Z. Chu, F. Zhou, P. Xiao, and N. Al-Dhahir, "Weighted sum rate optimization for STAR-RIS-assisted MIMO system," *IEEE Trans. Veh. Technol.*, vol. 71, no. 2, pp. 2122–2127, Feb. 2022.

[27] M. Grant, S. Boyd, and Y. Ye, "*CVX: Matlab Software for Disciplined Convex Programming*," 2008. [Online]. Available: http://cvxr.com/cvx/

[28] J. Nocedal and S. Wright, "*Numerical Optimization*. Springer Science & Business Media, 2006."

[29] Q. T. Dinh and M. Diehl, "Local convergence of sequential convex programming for nonconvex optimization," in *Recent Advances in Optimization and its Applications in Engineering*. Berlin, Germany: Springer, 2010.

[30] I. Pólik and T. Terlaky, *Interior Point Methods for Nonlinear Optimization*. Springer, 2010.

[31] Z. Zhou, N. Ge, Z. Wang, and L. Hanzo, "Joint transmit precoding and reconfigurable intelligent surface phase adjustment: A decomposition-aided channel estimation approach," *IEEE Trans. Commun.*, vol. 69, no. 2, pp. 1228–1243, Feb. 2021.

[32] Z. Wang, L. Liu, and S. Cui, "Channel estimation for intelligent reflecting surface assisted multiuser communications: Framework, algorithms, and analysis," *IEEE Trans. Wireless Commun.*, vol. 19, no. 10, pp. 6607–6620, Oct. 2020.

[33] C. Ruan, Z. Zhang, H. Jiang, J. Dang, L. Wu, and H. Zhang, "Approximate message passing for channel estimation in reconfigurable intelligent surface aided MIMO multiuser systems," *IEEE Trans. Commun.*, vol. 70, no. 8, pp. 5469–5481, Aug. 2022.

[34] A. Taha, M. Alrabeiah, and A. Alkhateeb, "Enabling large intelligent surfaces with compressive sensing and deep learning," *IEEE Access*, vol. 9, pp. 44 304–44 321, 2021.

[35] X. Yu, D. Xu, D. W. K. Ng, and R. Schober, "IRS-assisted green communication systems: Provable convergence and robust optimization," *IEEE Trans. Commun.*, vol. 69, no. 9, pp. 6313–6329, Sep. 2021.

[36] G. Zheng, K.-K. Wong, and T.-S. Ng, "Robust linear MIMO in the downlink: A worst-case optimization with ellipsoidal uncertainty regions," *EURASIP J. Adv. Signal Process.*, vol. 2008, no. 1, pp. 1–15, Jul. 2008.

[37] J. Wang and D. P. Palomar, "Worst-case robust MIMO transmission with imperfect channel knowledge," *IEEE Trans. Signal Process.*, vol. 57, no. 8, pp. 3086–3100, Aug. 2009.

[38] X.-D. Zhang, *Matrix analysis and applications*. Cambridge, U.K.: Cambridge Univ. Press,, 2017.

[39] Z.-Q. Luo, J. F. Sturm, and S. Zhang, "Multivariate nonnegative quadratic mappings," *SIAM J. Optim.*, vol. 14, no. 4, pp. 1140–1162, Jul. 2004.

[40] C. Pan, H. Ren, K. Wang, W. Xu, M. Elkashlan, A. Nallanathan, and L. Hanzo, "Multicell MIMO communications relying on intelligent reflecting surfaces," *IEEE Trans. Wireless Commun.*, vol. 19, no. 8, pp. 5218–5233, Aug. 2020.

Meng Shen is currently pursuing the Ph.D. degree with the School of Information Science and Technology, Southwest Jiaotong University, Chengdu, China. His current research interests include non-orthogonal multiple access, reconfigurable intelligent surface and physical layer security.

This article has been accepted for publication in IEEE Transactions on Communications. This is the author's version which has not been fully edited and content may change prior to final publication. Citation information: DOI 10.1109/TCOMM.2024.3430971

Xianfu Lei (Member, IEEE) is currently a Professor with the School of Information Science and Technology at Southwest Jiaotong University (SWJTU). He received the Ph.D. degree from SWJTU in 2012. From 2012 to 2014, he worked as a Research Fellow in the Department of Electrical and Computer Engineering at Utah State University. His research interests are in the fields of communication theory and wireless networks. He has published nearly 150 technical papers in scientific journals and international conferences. He was a recipient of the Best Paper Award at WCSP'18, IEEE ICCC'20, and IEEE Vehicular Technology Society Best Magazine Paper Award in 2023. He is serving as an Executive Editor for IEEE Communications Letters and an Editor for IEEE Transactions on Communications, IEEE Communications Magazine, and IEEE Wireless Communications Letters. He was an Area/Senior Editor for IEEE Communications Letters from 2019 to 2023. He also served as symposium/track and workshop chairs for major IEEE conferences including symposium chair for IEEE ICC'18.

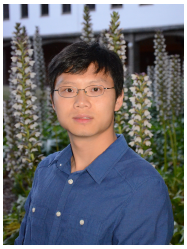

Xiangyun Zhou (Fellow, IEEE) is an Associate Professor at the Australian National University (ANU). He received the Ph.D. degree from ANU in 2010. His research interests are in the fields of communication theory and wireless networks. He has served as an Editor of IEEE TRANSACTIONS ON COMMUNICATIONS, IEEE TRANSACTIONS ON WIRELESS COMMUNICATIONS and IEEE WIRELESS COMMUNICATIONS LETTERS, and as an Executive Editor of IEEE COMMUNICATIONS LETTERS. He also served as symposium/track and workshop chairs for major IEEE conferences. He is a recipient of the Best Paper Award at ICC'11, GLOBECOM'22, ICC'24 and IEEE ComSoc Asia-Pacific Outstanding Paper Award in 2016. He was named the Best Young Researcher in the Asia-Pacific Region in 2017 by IEEE ComSoc Asia-Pacific Board. He is a Fellow of the IEEE.

George K. Karagiannidis (Fellow, IEEE) is currently Professor in the Electrical and Computer Engineering Dept. of Aristotle University of Thessaloniki, Greece and Head of Wireless Communications & Information Processing (WCIP) Group. He is also Faculty Fellow in the Artificial Intelligence & Cyber Systems Research Center, Lebanese American University. His research interests are in the areas of Wireless Communications Systems and Networks, Signal processing, Optical Wireless Communications, Wireless Power Transfer and Applications and Communications & Signal Processing for Biomedical Engineering. Dr. Karagiannidis is the Editor-in Chief of IEEE Transactions on Communications and in the past was the Editor-in Chief of IEEE Communications Letters. Recently, he received three prestigious awards: The 2021 IEEE ComSoc RCC Technical Recognition Award, the 2018 IEEE ComSoc SPCE Technical Recognition Award and the 2022 Humboldt Research Award from Alexander von Humboldt Foundation. Dr. Karagiannidis is one of the highly-cited authors across all areas of Electrical Engineering, recognized from Clarivate Analytics as Web-of-Science Highly-Cited Researcher in the nine consecutive years 2015-2023.